Published in final edited form as:
Nature. 2019 August 01; 572(7771): 609–613. doi:10.1038/s41586-019-1498-3.

Identification of an ATP-sensitive potassium channel in mitochondria

Angela Paggio[#1], **Vanessa Checchetto**[#2], **Antonio Campo**[1], **Roberta Menabò**[3], **Giulia Di Marco**[1], **Fabio Di Lisa**[1,3], **Ildiko Szabo**[2,3], **Rosario Rizzuto**[1,*], **Diego De Stefani**[1,*]

[1]Department of Biomedical Sciences, University of Padova, Via Ugo Bassi 58B, 35131 Padova, Italy

[2]Department of Biology, University of Padova, Via Ugo Bassi 58B, 35131 Padova, Italy

[3]CNR Institute of Neuroscience, Padova, Italy

[#] These authors contributed equally to this work.

Summary

Mitochondria provide chemical energy for endoergonic reactions in form of ATP. Their activity must meet cellular energy requirements, but mechanisms linking organelle performance to ATP levels are poorly understood. Here, we identify a mitochondria-localized protein complex that mediates ATP-dependent potassium currents, referred to as mitoK$_{ATP}$. We show that similarly to their plasma membrane counterparts, mitoK$_{ATP}$ channels are composed of pore-forming (MITOK) and ATP-binding (MITOSUR) subunits. In vitro reconstitution of MITOK together with MITOSUR recapitulates the main properties of mitoK$_{ATP}$. While MITOK overexpression triggers dramatic organelle swelling, its genetic ablation causes instability of mitochondrial membrane potential, widening of intracristal space and decreased oxidative phosphorylation. Most importantly, loss of Mitok suppresses cardioprotection elicited by diazoxide-induced pharmacological preconditioning. Our data indicate that mitoK$_{ATP}$ channels respond to the cellular energetic status by regulating organelle volume and function, thereby representing key players in mitochondrial physiology with potential impact on several pathological processes.

ATP-sensitive potassium channels (K$_{ATP}$) act as sensors of cellular metabolism. In the plasma membrane (pmK$_{ATP}$)[1] they couple cell excitability with energy availability[2,3]. They are also reported to be located to intracellular membranes, e.g. in mitochondria

[*]Corresponding authors: Contact information: Diego De Stefani, Department of Biomedical Sciences, University of Padova, Via Ugo Bassi 58/B, 35131 Padova, Italy, Phone: +390498276029, diego.destefani@gmail.com or Rosario Rizzuto, Department of Biomedical Sciences, University of Padova, Via Ugo Bassi 58/B, 35131 Padova, Italy, Phone: +390498273001, rosario.rizzuto@unipd.it.

Author contributions

F.D.L. designed and discussed I/R experiments. R.M. and G.D.M. performed and analyzed I/R experiments. I.S. designed electrophysiological study. V.C. performed recordings, and I.S. and V.C. analyzed biophysical data. R.R. and D.D.S designed and supervised all other experiments. A.P., A.C. and D.D.S. performed all other experiments and analyzed data. I.S., R.R. and D.D.S conceived the study, discussed all the results and wrote the manuscript.

Author information

All authors declare no competing interests.

Europe PMC Funders Author Manuscripts

(mitoK$_{ATP}$)[4,5], but in this context their existence is a matter of debate[6]. mitoK$_{ATP}$ mediates the electrophoretic uptake of potassium (K^+), driven by the negative mitochondrial membrane potential ($\Delta\psi_m$), and it is inhibited by physiological ATP levels. MitoK$_{ATP}$ was first described in the early 90s through patch clamp of mitoplasts[4] or by partial purification techniques[5]. Since then, the mitoK$_{ATP}$ has been characterized from the pharmacological point of view, and both openers (i.e. diazoxide) and inhibitors (i.e. sulphonylureas and 5-hydroxydecanoate, 5-HD) have been described, some of them with proposed specific action on mitoK$_{ATP}$ versus pmK$_{ATP}$ [7]. Drugs targeting K$_{ATP}$ channels are useful in several pathologies. Importantly, some of their uses are due to the modulation of pmK$_{ATP}$ [8], but others seem to depend on their effects on mitoK$_{ATP}$. For instance, pharmacological preconditioning with diazoxide efficiently protects the heart from ischemia reperfusion injury[9,10], even in the absence of cardiac pmK$_{ATP}$ [11,12]. However, the molecular identity and genuine pharmacology of this channel remain elusive[7,13,14].

MITOK is a cation channel

We screened a subset of mitochondrial proteins with unknown function and focused on a candidate encoded by the *CCDC51* gene (NCBI ID 79714), hereafter named *MITOK*, whose overexpression profoundly impaired mitochondrial physiology. The *MITOK* gene is conserved in vertebrates, where it encodes a unique 45 kDa protein with a predicted N-terminal mitochondrial targeting sequence (MTS), one coiled coil and two transmembrane domains. In humans the *MITOK* gene encodes for two isoforms: isoform 1 (full-length but no predicted MTS) and isoform 2, a splice variant lacking the first 109 aa (34 kDa) with a supposed MTS (Figure 1a). Analyses of RNA and protein levels using existing datasets revealed that *MITOK* is expressed in all tissues in humans and mice[15,16]. First, we experimentally validated the mitochondrial localization of MITOK in humans and mice. Immunofluorescence shows full co-localization with a mitochondrial marker in HeLa cells (Figure 1b) and subcellular fractionation of mouse liver revealed a progressive enrichment of Mitok in mitochondria and mitoplasts, and absence on the outer membrane (Figure 1c). Carbonate extraction confirmed membrane insertion (Extended data figure 1a), indicating that MITOK is in the IMM. To investigate its topology, we exploited two antibodies, one against the N-terminal half and the other covering the C-terminal half (Figure 1d). Proteinase K digestion of mitoplasts caused the loss of full length Mitok and the appearance of a smaller fragment recognized by the N-terminal antibody (Extended data figure 1b), indicating that a portion of the protein is protected inside the organelle. Conversely, no residual signal was detected with an antibody against the region between the two TM domains, indicating that this part is exposed to the intermembrane space (IMS). Overall, MITOK is a two-pass protein of the IMM with both the N- and C-termini exposed toward the matrix. Next, we cloned and tagged (-Flag, -V5 and -GFP) murine Mitok and investigated the effect of its overexpression. In terms of morphology, Mitok overexpression causes organelle fragmentation (Extended data figure 1c) and swelling (Figure 1e). At functional level, Mitok overexpression caused a drop in $\Delta\psi_m$ (Extended data figure 1d) and agonist-induced mitochondrial Ca^{2+} uptake, i.e. an additional readout for changes in $\Delta\psi_m$ (Extended data figure 1e). As to human isoforms, we designed both specific (isoform 1 vs isoform 2) and non-specific (pan-isoforms) primers for qPCR. Both isoforms can be

detected in HeLa cells at transcript level, although isoform 2 is 10 times less expressed (Extended data Figure 1f). Despite this, only a single band can be detected in Western blots using HeLa cells (Extended data Figure 1g). In most of human tissues, isoform 1 shows good expression, while isoform 2 is barely detectable. This pattern is reversed in the case of spleen, with significant expression of isoform 2 and marginal expression of isoform 1 (Extended data Figure 1f). As to their role, isoform 1 localizes to mitochondria and its overexpression induced, similarly to murine Mitok, morphological and functional organelle impairment (Extended data Figure 2a-b), indicating that both mouse and human *MITOK* genes encode for similar proteins, although some human cells express a shorter and less active splicing variant. Overall, MITOK overexpression causes a severe perturbation of mitochondrial structure and function. Although several mechanisms could account for these effects, we reasoned that MITOK could act as a cation channel, given that valinomycin, a K^+ ionophore (i.e. a molecule mediating K^+ influx into the matrix), closely mimics the observed phenotype.

Unambiguous demonstration of channel activity necessarily requires a simplified reconstitution approach using recombinant proteins. We thus measured Mitok channel activity in the planar lipid bilayer using Mitok from two systems, *E. coli* and the wheat-germ cell-free transcription/translation tool, both expressing Mitok at high levels (Extended data figure 3a-b). We observed channel activity in a medium containing only K^+ as cation (Figure 1g-h). Burst-like, flickering activity and cooperative transition between dual- or multi-states were observed (Extended data figures 3c-d)[4,17]. The channel showed an ohmic behavior (Extended data figure 3e), was voltage-independent (Extended data figure 3f) and was selective for K^+ over chloride (P_K:P_{Cl}=1:0.02, Extended data figure 3g). Channel conductance was 57 ± 11 pS in both 100 mM KCl and K-gluconate media (Figure 1h and Extended data figure 3e)[18,19]. Channel activity could be blocked by addition of Barium, an inhibitor of K^+ channels (Extended data figure 3h), but not by paxilline, an inhibitor of the BK_{Ca} channels (Extended data figure 3i).

MITOK and MITOSUR form the mitoK$_{ATP}$ channel

Based on these data, we pursued the hypothesis that it could be mitoK$_{ATP}$, despite the fact that i) similarly to the lysosomal K^+ channel TMEM175[20], MITOK does not harbor the typical K^+ selectivity filter (accordingly, it allows permeation of Na^+, see Extended data figure 4a), and ii) the purified protein per se did not respond to ATP (Extended data figure 4b) or 5-HD (Extended data figure 4c). However, we reasoned that ATP sensitivity could be conferred by a regulatory SUR-like subunit. Ten different ATP-Binding Cassette (ABC) proteins can be detected in mitochondria[15], most belonging to ABCB subfamily[21]. We focused on ABCB8, hereafter named MITOSUR, since i) its tissue expression best correlates with MITOK, and ii) it was suggested to be part of mitoK$_{ATP}$ [22]. We expressed *in vitro* Mitok together with MITOSUR, that were folded and incorporated into liposomes, as indicated by thermal stability assay (Extended data figure 5a-c) and membrane extraction (Extended data figure 5d), with a membrane orientation resembling that in mitoplasts (Extended data figures 5e-f and see later). Mitok and MITOSUR were able to form a K^+ permeable channel (Figure 2a and Extended data figures 5g-i) that was i) inhibited by mM concentrations of ATP, ii) activated by diazoxide (Figures 2a, Extended data figure 5g-h),

and iii) blocked by both the sulphonylurea glibenclamide (Figure 2b), and 5-HD (Figure 2c). The channel conductance slightly decreased upon addition of 1 mM Mg^{2+} (Extended data figure 5j). Activity was observed in the absence of divalent cations (Extended data Figure 5k) and in Na^{+} (Extended data Figure 5l). Overall, all these features recapitulate the fundamental electrophysiological properties and the consensus pharmacological profile of mitoK$_{ATP}$ [18,19], with MITOK forming the K^{+}-permeant channel and MITOSUR acting as a modulatory subunit carrying the ATP-binding site. We next investigated its membrane topology by performing protease protection assay using an antibody covering the ATP-binding region (aa 394-693). Extended data figure 6a shows that proteinase K leads to the loss of MITOSUR-specific band, indicating that the ATP-binding cassette is exposed to the IMS. Overall, membrane orientation of both MITOK and MITOSUR are supported by previous bioenergetics studies[5] and independent proteomic approaches[23].

In light of this architecture, we reasoned that the unregulated K^{+} uptake in the cells overexpressing Mitok alone must be the cause of organelle impairment (Figure 1). If this is true, the combined overexpression of Mitok and MITOSUR should reverse mitochondrial dysfunction. To test this, we first verified the physical interaction between Mitok and MITOSUR through co-immunoprecipitation (Figure 3a). In addition, immunoblot analysis of digitonin-solubilized mitochondrial complexes in native conditions revealed an approximately 500 kDa band reacting with both MITOK and MITOSUR antibodies (Figure 3b), a size compatible with an octamer (4 MITOK and 4 MITOSUR). Accordingly, immunoprecipitation of endogenous MITOK could efficiently pull down MITOSUR using both murine and human mitochondria (Figure 3c and Extended data figure 6b). As to their function, overexpression of Mitok alone caused a significant decrease of both these parameters (Figures 3d-e), while overexpression of the MITOSUR subunit alone did not affect organelle functions. Most importantly, the combined overexpression of the two subunits fully rescued $\Delta\psi_m$ and Ca^{2+} dynamics (impaired by Mitok alone), suggesting the recovery of the proper channel gating. We also generated a MITOSUR mutant (MITOSUR^{K513A}) unable to bind ATP. This mutant could still interact with Mitok (Extended data figure 6c) but failed to respond to ATP in electrophysiological experiments (Figure 3f), to rescue the loss of mitochondrial membrane potential and Ca^{2+} accumulation caused by Mitok overexpression (Figures 3d-e), further confirming that ATP acts as channel inhibitor. Overall, our data indicate that MITOK and MITOSUR form a complex responsible for the ATP-sensitive mitochondrial K^{+} transport both *in vitro* and *in situ*.

MITOK controls mitochondrial volume

Despite the agreement on the cytoprotective role of mitoK$_{ATP}$ opening in stress conditions (mainly based on pharmacological studies)[10], its constitutive physiological function remains obscure. We thus generated HeLa cells knockout for *MITOK* (HeLa$^{MITOK\text{-}KO}$) by Crispr/Cas9 DNA cleavage, using two different guides (Extended data Figure 7a-b). We first confirmed the idea that MITOK is required for ATP-dependent K^{+} fluxes in mitochondria, by measuring mitochondrial swelling rates in a K^{+}-based buffer[9,24]. In isolated wild type mitochondria, ATP decreases and diazoxide increases the swelling rates, through the inhibition and activation the mitoK$_{ATP}$, respectively (Figure 4a). Accordingly, mitochondria

isolated from *MITOK*-KO cell lines swell at a constant rate, independently of either ATP or diazoxide (Figure 4b).

MITOK-KO cells were viable and showed a highly interconnected mitochondrial network by optical microscopy. Although gross morphology appeared similar, ablation of *MITOK* led to the appearance of several doughnut-shaped (toroidal, ring-like) mitochondria (Extended data figure 7c), a phenotype associated with impaired organelle K^+ homeostasis[25]. $\Delta\psi_m$ was intact, but HeLa$^{MITOK\text{-}KO}$ cells undergo asynchronous, rapid and transient depolarizations of single mitochondria (Extended data figures 7d-e), a phenomenon known as mitochondrial "flickering" or "flashes"[26–29]. Importantly, this phenotype is specific, since the reintroduction of Mitok and MITOSUR restored the $\Delta\psi_m$ stability (Figure 4c). In terms of oxidative performance, ablation of *MITOK* caused a decrease of basal and maximal oxygen consumption rate (OCR), despite similar expression of electron transport chain components (Figure 4d and Extended data figure 7f). Again, this could be partially rescued by i) pharmacological treatment with a minimal dose of valinomycin (i.e. having no effect in control cells) (Extended data figure 8a) and ii) reintroduction of Mitok and MITOSUR (Extended data figure 8b). To understand the causes of altered organelle function, we investigated mitochondrial ultrastructure by TEM. Although gross mitochondrial morphology was preserved, *MITOK*-KO cells show enlarged cristae (Figure 4e), in line with the effect of the inhibition of another IMM K^+ channel[30]. Normal cristae morphology was readily restored by re-expression of mitoK_{ATP} (Figure 4e). Given that K^+ fluxes across the IMM are the main determinants of organelle water content[31], we speculated that cristae remodeling could be due to a dysregulation of matrix volume, as suggested by swelling experiments (Figures 4a-b). Indeed, the IMM rapidly rearranges in response to osmotic changes, with matrix contraction leading to expanded cristae, and matrix swelling causing the collapse of the intracristae compartment. Accordingly, genetic ablation of *MITOK* caused both widening of intra-cristae space (Extended data figure 8c) and lower oligomerization of OPA1 (an additional biochemical readout for cristae remodeling, where higher multimerization correlates with tighter cristae[32]). Even in these cases, valinomycin partially recovered normal cristae morphology (Extended data figure 8c-d).

We then wondered how mitoK_{ATP} affects organelle adaptations to energy stress. We thus treated wt and *MITOK*-KO cells with the glycolysis inhibitor 2-deoxyglucose (2DG), that rapidly decreases global cellular metabolism (Extended data figures 8e-f). First, we tested how mitochondrial morphology changes in response to ATP depletion. Wild type HeLa cells rapidly underwent to fragmentation of the mitochondrial network (Figure 4f). Conversely, metabolic inhibition in *MITOK*-KO cells caused no evident change of the overall mitochondrial morphology (Figure 4f), indicating that mitochondrial morphology promptly adapts to the energetic state of the cells through a mitoK_{ATP}-dependent mechanism. Then, we monitored ROS production during metabolic stress and/or pharmacological modulation of mitoK_{ATP}. Extended data figure 8g indicates that: i) loss of *MITOK* increases ROS production, notwithstanding the decreased OCR, further supporting the latent mitochondrial dysfunction; ii) diazoxide increases ROS in wild type but not in MITOK-KO cells, supporting the idea of mitoK_{ATP} as a regulator of redox state; iii) metabolic stress can increase ROS production in control cells, while iv) ROS levels marginally increase when

mitoK$_{ATP}$ is absent, thus indicating that mitochondria K^+ homeostasis impinges on the regulation of redox balance during metabolic stress. Overall, our data indicate that mitoK$_{ATP}$ regulates mitochondrial adaptation to cellular stress possibly through the regulation of matrix volume (Figure 4g). In addition, loss of *MITOK* increases cell death triggered by oxidative stress (Extended data Figure 8h), as suggested by others[33] and in line with cristae widening[34].

MITOK is required for pharmacological preconditioning

Finally, we generated *Mitok*-KO mice through specific deletion of exon 4, containing most of the coding sequence. Overall, these mice show no overt phenotype (born at the expected Mendelian ratio, similar aspect and weight gain), at least until 4 months of age. To demonstrate the lack of mitoK$_{ATP}$ activity, we measured organelle K^+ fluxes using $^{86}Rb^+$ as surrogate[18]. Energized mitochondria isolated from wild type livers showed ATP- and diazoxide-sensitive K^+ uptake (Figure 5a). Conversely, neither ATP nor diazoxide were able to alter K^+ fluxes when Mitok was absent (Figure 5b-c). Finally, we performed ex vivo ischemia/reperfusion (I/R) experiments in wild type and Mitok-KO mice and evaluated the cardioprotective effect triggered by pharmacological preconditioning (PPC) induced by diazoxide. As shown in Figures 5d, untreated Mitok-KO hearts are slightly more sensitive to I/R protocol, further confirming the cytoprotective role of Mitok. As already shown[10,12,35,36], diazoxide PPC efficiently protects the heart from reperfusion damage. Most importantly, PPC is nearly lost in Mitok-KO hearts, as evidenced also by analysis of infarct size (Figure 5e), thus demonstrating that mitoK$_{ATP}$ is the molecular target of diazoxide, at least in this pathological setting.

In conclusion, we have identified a novel protein complex accounting for ATP-sensitive K^+ transport across the IMM, composed of a channel forming subunit (MITOK) and a regulatory subunit carrying the ATP-binding domain (MITOSUR). Although we do not exclude that other proteins could exert similar activities in specific tissues[37], in vitro reconstitution of this complex is sufficient to reliably recapitulate the main electrophysiological properties and pharmacological profile of the long-sought mitoK$_{ATP}$ [13]. Overall, the here identified mitoK$_{ATP}$ stands as a new player in mitochondrial physiology, representing a potential mechanism to match ATP availability to energy production and thus contributing to the homeostatic control of cellular metabolism during stress condition.

Methods

Chemicals, cell culture and transfection

All chemicals were purchased from Sigma-Aldrich, unless otherwise specified. All the experiments were performed in HeLa cells (ATCC Number: CCL-2) cultured in Dulbecco's modified Eagle's medium (DMEM) (Gibco #41966052, Thermo Fisher Scientific), supplemented with 10% fetal bovine serum (FBS) (Thermo Fisher Scientific), containing penicillin (100 U/ml) and streptomycin (100μg/ml) (Euroclone). When needed, cells were seeded onto 13- or 24-mm glass coverslips and allowed grow to 50% confluence before transfection. Transfection was performed with standard Ca^{2+}-phosphate procedure.

Europe PMC Funders Author Manuscripts

Constructs

Murine Mitok coding sequence (NCBI ID: NM_025689) was amplified from mouse skeletal muscle cDNA library by PCR using the following primers.

For the cloning of Mitok-GFP: fw,5'-CTCGAGATGACAGGGTGCAGCCCCGT-3'; rv, 5'-GGATCCCGACTGGTCTTGAACAGCATGT-3'. The PCR fragment was cloned into pEGFP-N1 (Clontech) using XhoI and BamHI sites.

For the cloning of Mitok-Flag into pcDNA3.1: fw, 5'-AAGCTTATGACAGGGTGCAGCCCCGT-3'; rv, 5'-CTCGAGTTACTTATCGTCGTCATCCTTGTAATCACTGGTCTTGAACAGCATGT-3'. The PCR fragment was cloned into pcDNA3.1 (Thermo Fisher Scientific) using HindIII and XhoI sites.

For the cloning of Mitok-V5 into pcDNA3.1: fw,5'-AAGCTTATGACAGGGTGCAGCCCCGT-3'; rv,5'CTCGAGTTACGTAGAATCGAGGAGACCGAGAGGGTTAGGGATAGGCTTACCACTGGTCTTGAACAGCATGT-3'. The PCR fragment was cloned into pcDNA3.1 using HindIII and XhoI sites.

For the cloning of Mitok-6xHis in pIVEX1.3WG: fw,5'-CCATGGCAACAGGGTGCAGCCCCGTGTT-3'; rv, 5'-CTCGAGACTGGTCTTGAACAGCATGT-3'. The PCR fragment was cloned into pIVEX1.3WG (Roche) using NcoI and XhoI sites.

For the cloning of Mitok-6xHis in pET-28A (+): fw,5'-AAGCTTGCATGACAGGGTGCAGCCCCGT-3'; rv, 5'-CTCGAGTTAACTGGTCTTGAACAGCA-3'. The PCR fragment was cloned into pET-28A(+) (Novagen) using HindIII and XhoI sites.

Human MITOK coding sequences (NCBI ID: NM_001256964 and NM_001256965) were amplified from human spleen cDNA library by PCR using the following primers.

For the cloning of hs-MITOK-iso1 (NM_001256964) into pcDNA3.1: fw,5'-GGATCCATCTCAGGATGATGGGGC-3'; rv,5' GAATTCTTAGCTGGCTTTGAATAGCATGTAGAG-3'. The PCR fragment was cloned into pcDNA3.1 using BamHI and EcoRI sites.

For the cloning of hs-MITOK-iso1-HA into pcDNA3.1: fw,5'-GGATCCATCTCAGGATGATGGGGC-3'; rv,5' GAATTCTTAAGCGTAATCTGGAACATCGTATGGGTAGCTGGCTTTGAATAGCATGTAGAG-3'. The PCR fragment was cloned into pcDNA3.1 using BamHI and EcoRI sites.

For the cloning of hs-MITOK-iso2 (NM_001256965) into pcDNA3.1: fw,5'-GGATCCGCCACCATGGTGGCTCGAGGGCTTG-3'; rv,5' GAATTCTTAGCTGGCTTTGAATAGCATGTAGAG-3'. The PCR fragment was cloned into pcDNA3.1 using BamHI and EcoRI sites.

For the cloning of hs-MITOK-iso2-HA into pcDNA3.1: fw,5'-GGATCCGCCACCATGGTGGCTCGAGGGCTTG-3'; rv,5' GAATTCTTAAGCGTAATCTGGAACATCGTATGGGTAGCTGGCTTTGAATAGCATGTAGAG-3'. The PCR fragment was cloned into pcDNA3.1 using BamHI and EcoRI sites.

MITOSUR expression plasmid (pCMV6-ABCB8-myc-Flag), containing the NM_007188 reference sequence (and corresponding to ABCB8 transcript variant 2), was purchased from Origene (cat no RC224948).

For the cloning of MITOSUR in pIVEX1.3WG:c fw,5'-GCGATCGCCCATATGCTGGTGCATTTA-3'; rv,5'-CTACCGAGTACTTTAAACCTTATC-3'. The PCR fragment was cloned into pIVEX1.3WG using NdeI and ScaI sites.

The generation of the MITOSUR^{K513A} mutant was performed by mutagenesis PCR using the wild type mitoSUR encoding vector as template and the mutagenesis primer: 5'-GGCCAGTCTGGCGGAGGAGCGACCACCGTGGCTTCCCTG-3'. Please note that amino acid numbering refers to ABCB8 isoform 1 (Uniprot ID Q9NUT2).

For the generation of the construct MITOSUR-Myc-P2A-Mitok-Flag in pcDNA3.1, MITOSUR-Myc was amplified with following primers: fw, 5'-GGATCCATGCTGGTGCATTTATTTCG -3'; rv, 5'-GAATTCCGGTCCAGGATTCTCTTCGACATCTCCGGCTTGTTTCAGCAGAGAGAAGTTTGTTGCCAGATCCTCTTCTGAGATGAGTTTCTGCTCGGACTTGTGCTGGTGGCTCC -3'. The PCR fragment was cloned into pcDNA3.1 using BamHI and EcoRI sites.

Mitok-Flag was amplified with the following primers: fw, 5'-GAATTCATGACAGGGTGCAGCCCCGT-3'; rv, 5'-GCGGCCGCTTACTTATCGTCGTCATCCTTGTAATCACTGGTCTTGAACAGCATGT-3'. The PCR fragment was cloned into the above-mentioned plasmid using EcoRI and NotI sites.

For the generation of mitochondrial-targeted mEmerald, mEmerald was amplified from the mEmerald-Mito-7 plasmid (Addgene plasmid #54160), a kind gift of Michael Davidson, with the following primers: fw, 5'- AAGCTTGTGAGCAAGGGCGAGG-3'; rv, 5'-GAATTCTTACTTGTACAGCTCGTCCATG-3'. The PCR fragment was cloned in a custom pcDNA3.1 plasmid containing four repeated mitochondrial targeting signals from human COX8A (pcDNA3.1-4mt) using HindIII and EcoRI sites.

All constructs were verified by Sanger sequencing.

RNA extraction, reverse transcription and quantitative real time PCR

For qPCR analyses, HeLa cells were lysed in an appropriate volume of TRIZOL reagent (Thermo Fisher Scientific). For human tissues, a commercial mRNA library was used (Clontech Human Total RNA Master Panel II, cat no. 636643). The RNA was quantified with a NanoDrop (Thermo Fisher Scientific). Complementary DNA was generated with a cDNA synthesis kit (SuperScript II, Thermo Fisher Scientific) using oligo(dT)12-18 primer

(Thermo Fisher Scientific) and analyzed by real-time PCR using the SYBR green chemistry (Thermo Fisher Scientific). Primer were designed using Primer-BLAST[38]. Real-time PCR standard curves were constructed by using serial dilutions of cDNAs of the analyzed samples, using at least four dilution points and the efficiency of all primer sets was between 80 and 120%. The housekeeping gene *ACTIN* were used as an internal control for cDNA quantification and normalization of the amplified products. All data are reported as mean ± s.d., with $n = 3$. In the case of HeLa cells, 3 independent RNA extractions and RT reactions were used. In the case of human tissues, 3 technical replicates were used. qPCR primer sequences were as follows:

hsMITOK-Pan-FW: GGATGCTGCAGGAGGAGAAG

hsMITOK-Pan-RV: CTTGGTCCTCTCAGCCCTTG

hsMITOK-Iso1-FW: CGGAACCGTAGGAGGGGTACT

hsMITOK-Iso1-FW: CTCCGAACCAGTACGTGGGG

hsMITOK-Iso2-FW: CGGTTTTCTCTTTGCAGGCT

hsMITOK-Iso2-RV: TCTTGGTCCTCTCAGCCCTT

hsACTIN-FW: CCTTTTATGGCTCGAGCGGC

hsACTIN-RV: CATCATCCATGGTGAGCTGGC

Please note that isoform-specific primers are not very efficient compared to non-specific ones (see Extended Data Figure 1d), most likely due the fact that 5'UTR region is under-represented when using oligo-dT for RT (all primers are however specific, since they fail to detect significant transcripts in HeLa$^{mitoK\text{-}KO}$ cells).

Expression and purification of Mitok and of MITOSUR

C41(DE3) *E. coli* cells were transformed with the Mitok-expressing plasmid. Expression was achieved as described in [39]. Five hours after induction with IPTG, cells were collected and sonicated in 250 mM NaCl and 25 mM TRIS, pH 8.0, with 1 μg/ml leupeptine and pepstatine. The samples were subsequently centrifuged 15000x*g* for 30 min at 4°C to separate the membrane fraction (pellet) from the soluble fraction (supernatant). Then, the pellet was solubilized in 2.5% decyl-β-D-maltopyranoside (Sigma-Aldrich) in the sonication buffer for 3 hours, and the resulting soluble material was loaded onto Ni resin (HIS-Select Nickel Affinity Gel, Sigma-Aldrich). After 3 washes in equilibration buffer (50 mM sodium phosphate, pH 8.0, 300 mM sodium chloride), Mitok was eluted with a 250 mM imidazole solution in equilibration buffer. All fractions were collected and tested using standard SDS-PAGE and Western blot analyses. Immuno-detection of the expressed channel was performed using anti-His6 tag antibody (Sigma-Aldrich) and anti-MITOK antibody. For *in vitro* expression and electrophysiology the protocol described in [40] was used. Briefly, Mitok and MITOSUR proteins were expressed either separately or together in an *in vitro* wheat (*Triticum aestivum*) germ lysate system based on the continuous exchange cell-free

technique, using the Wheat Germ CECF Kit (Roche). Synthesis was achieved for 24 h at 24°C under continuous mixing on a Thermomixer comfort unit (Eppendorf). After expression, the reaction mixture was either loaded on Ni-chromatography column or directly solubilized for 30 min with either Triton X-100 or digitonin (1% w/v). No differences were observed in channel activity depending on the detergent used. Following centrifugation, the supernatant containing the solubilized proteins was diluted 1:10 in 10 mM HEPES, pH 7.4. For co-expression experiments, 1:1 ratio of DNA was used. After expression, Mitok alone or the Mitok and MITOSUR reaction mix were solubilized with 1% Triton X-100 or digitonin and incorporated into liposomes. Purified soybean asolectin was used to produce liposomes at 2 mg/ml in 10 mM HEPES, 10 mM $CaCl_2$, pH 7.3. After solubilization, the reaction mix was incubated with liposomes for 15′ at RT. Liposomes were pelleted and suspended in the same volume and subjected to alkaline extraction by adding 1/10 volume of 2 M Na_2CO_3 in order to check for insertion of the proteins into the liposomes (not shown). Liposomes harboring the proteins were frozen in small aliquots and used for one day after thawing.

Electrophysiological recording of Mitok and Mitok+MITOSUR activities in planar lipid bilayer and data analysis

A Warner Instruments (Hamden, CT, USA) BC-525C electrophysiological planar bilayer apparatus was used. Bilayers with a capacity of approximately 150 to 200 pF were prepared using partially purified (by precipitation with cold acetone from a chloroform solution) asolectin solution in decane/chloroform with a 100:1 ratio per mg of lipids (Sigma) across a 250 μm hole in a polystyrene cuvette. The contents of both chambers were stirred by magnetic bars when necessary. Voltages reported are those of the cis chamber, and current is considered positive when carried by cations flowing from the cis compartment to the trans compartment. Three ml of recording solution were added to both compartments. 100 mM K-gluconate, 10 mM HEPES/KOH, pH 7.4 or 100 mM KCl, 10 mM HEPES/KOH pH 7.4 medium ($[K^+]$ 117 mM) were used unless otherwise specified. Lack of activity in the membrane before addition of the protein was monitored for at least 5 minutes in each experiment and long-lasting (≥30 minutes) control experiments showed no activity without addition of the protein (n=50) or following addition of the detergent only (at the same concentration that is added with the proteins, n=15). Ten μL of the solubilized and diluted (1:10, see above) Mitok or Mitok+MITOSUR mixture incorporated into liposomes were added to the cis side. The final detergent concentration was between 0.0003 and 0.0006%. Channel modulators were added to both compartments to the required concentration for inhibition or activation assays. Electrical connections were made using Ag/AgCl electrodes and agar salt bridges to minimize liquid junction potentials. The current was digitized at a sampling rate of 10 kHz, the signals were filtered at 500 Hz and the data were analyzed offline using pCLAMP8.0 (Molecular Devices, Sunnyvale, CA, USA). The channel recordings illustrated are representative of the most frequently observed amplitudes of the opening channels under a given condition. The conductance values were calculated from the current-voltage relationship, averaged from at least three independent experiments. P(open) was calculated from segments of continuous recordings lasting 60 s. Amplitude histograms were obtained from ≥30 s gap-free current traces. Number of events in the amplitude histograms refer to the number of binned points at a given amplitude in the recordings. P_K/P_{Cl}, ratios were calculated from the measured reversal potentials using the Goldman-

Hodgkin-Katz equation taking into account the effective [K^+] (117 mM trans versus 287 mM cis). All analysis was performed without leak subtraction and current trace idealization. Analysis and fitting of data was performed using Origin 6.1 programs (for Gaussian and linear fitting).

Thermal aggregation assay

The thermal aggregation profile of MITOSUR and Mitok proteins has a been obtained by an adaptation of cellular thermal shift assay to *in vitro* protein expression mixtures[41]. Briefly, WGL lysate was solubilized in 0,8% digitonin then treated for 30 minutes at RT in agitation with 1 mM ATP and 2 mM $MgCl_2$ to avoid the interference of any chaperone or folding helper components in the wheat germ extract used for protein expression. WGL lysate has been aliquoted into PCR-tubes in equal volumes (40 ul) and each sample incubated at a different temperature, covering the interval between 37 and 95 °C. A reference sample treated analogously was stored at 4°C and has been used for densitometry values normalization. Each sample has been exposed to the designed temperature for 10 min through an Eppendorf 96-well thermal cycler, vortexed and centrifuged 30,000x*g* for 25 min at 4 °C to pellet aggregated and denatured proteins. Each supernatant containing the soluble proteins fraction has been carefully removed and transferred into a new tube. The soluble fraction has been analyzed and quantified for each temperature of the gradient using Western blotting technique, loading an equivalent volume of each sample into the wells of gel, and blotted using the indicated antibodies. The samples for each CETSA melt curve have been run on the same gel. All experiments were performed at four independent occasions, and data are given as the average from these experiments. The solid lines represent the best fits of the data using a Boltzmann sigmoidal fitting within the GraphPad Prism software.

Generation of MITOK-KO cells

For the generation of MITOK-KO cell lines, two Cas9 guides targeting different regions of the human *MITOK* gene were designed (GCCCCTCCGAACCAGTACGT and TCATGAGAAGGAGCGCACAA) using the MIT Crispr design tool[42], and cloned into the BsmBI site of the pLentiCrisprV2 plasmid, a kind gift of Feng Zhang (Addgene plasmid #52961)[43]. Lentiviral particles were produced by transfecting 293T cells with the transfer plasmids together with pRSV-Rev (Addgene plasmid #12253), pMDLg/pRRE (Addgene plasmid #12251) and pMD2.G (Addgene plasmid #12259) plasmids, kindly provided by Didier Trono. Three days after transfection, the supernatants were collected, centrifuged and cleared through 0.45μm cellulose acetate filters. Target cells were infected with viral particles and selected with one μg/ml puromycin for one week. Dilution cloning was performed to obtain different monoclonal cell populations that were screened and validated for *MITOK* gene ablation through Western blot.

Antibodies, SDS-PAGE and Western blot

Cells were lysed in RIPA buffer (150 mM NaCl, 25 mM Tris-Cl pH 8, 1 mM EGTA-Tris, 1% Triton X-100, 0.5% sodium deoxycholate and 0.1% SDS) supplemented with Complete EDTA-free protease inhibitor mixture (Roche Applied Science) and PhosStop (Roche Applied Science) for 30 minutes on ice. Crude extracts were centrifuged 15000x*g* for 10 minutes to remove debris, and proteins in the supernatant were quantified using the BCA

Protein Assay Kit (Pierce). 30 μg of proteins were dissolved in LDS sample buffer (Life Technologies) supplemented with 100 mM dithiothreitol, heated for 5 minutes at 90°C and loaded on 4-12% Bis-Tris NuPage gels (Thermo Fisher Scientific). After electrophoretic separation, proteins were transferred onto nitrocellulose membranes by wet (Thermo Fisher Scientific) or semidry (BioRad) transfer. Membranes were blocked for 1 hour at RT with 5% non-fat dry milk (BioRad) in TBS-T (50 mM Trizma, 150 mM NaCl and 0.1% Tween) and probed with the indicated primary antibodies over night at 4°C. Isotype matched, horseradish peroxidase-conjugated secondary antibodies (BioRad) were used followed by detection by chemiluminescence (SuperSignal Pico, Pierce). The following primary antibodies were used: anti-MITOK$_{C\text{-}term}$ (1:1000, Sigma HPA011408), anti-MITOK$_{N\text{-}term}$ (1:10000, Sigma HPA010980), anti-MCU (1:1000, Sigma HPA016480), anti-MICU1 (1:1000, Sigma HPA037480), anti-HSP60 (1:5000, Santa Cruz sc-1052), anti-OPA1 (1:1000, BD biosciences 612606), anti-MITOSUR (1:1000, Abcam ab182662), anti-OXPHOS (1:1000, Abcam ab110413), anti-TOM20 (1:10000, Santa Cruz sc-11415), anti-Flag (1:1000, Cell Signaling #2368). Western blots are representative of at least three independent preparations. Where needed, uncropped images of Western blots used for the assembly of final figures are provided in Supplementary Figure 1.

Blue Native PAGE

Mitochondrial fractions were lysed in the appropriate volume of NativePAGE Sample Buffer (Thermo Fisher Scientific) supplemented with 3% (w/w) digitonin. Crude extracts were centrifuged at 15000x*g* for 10’ to remove debris, and proteins in the supernatant were quantified using the BCA Protein Assay Kit (Pierce). 100 μg of proteins were dissolved in NativePAGE sample buffer supplemented with Comassie G-250 (Thermo Fisher Scientific) and loaded on a 4-16% Novex NativePAGE Bis-Tris Gel System (Thermo Fisher Scientific). After electrophoretic separation, proteins were transferred onto PVDF membranes and probed with the indicated antibodies. As molecular weight marker, NativeMark Unstained Protein Standard (Thermo Fisher Scientific) was used and stained with Colloidal Blue Staining Kit (Thermo Fisher Scientific). Isotype matched, horseradish peroxidase-conjugated secondary antibodies (BioRad) were used followed by detection by chemiluminescence (SuperSignal Pico, Pierce).

Mitochondrial isolation, proteinase K protection and swelling assays

Mitochondria were isolated from HeLa cells or mouse liver through differential centrifugation as previously described[44]. Mitoplasts were obtained through osmotic swelling by incubating mitochondrial fraction in 20 mM Tris-Cl pH 7.4 for 20 minutes on ice. The same amount of mitoplasts was treated with proteinase K (100 μg/mL) at 4°C for the indicated time and the proteolytic reaction was quenched by PMSF addition. Samples was then loaded on SDS-PAGE and processed for Western blot as described above. Results are representative of at least two different proteolytic reactions.

For swelling assay, mitochondria were isolated using a slightly modified protocol to accelerate the procedure (as reported, mitoK$_{ATP}$ activity degrades quickly after organelle isolation). HeLa cells were initially disrupted through a brief (4 seconds) sonication (using a braun Labsonic P at full cycle and 30% amplitude). After differential centrifugation, 0.25

mg of mitochondria were suspended in a cuvette containing 2 ml of swelling assay buffer (100mM KCl, 20 mM HEPES, 1 mM $MgCl_2$, 2 mM Pi, 1 mM EGTA, 0.1% BSA, 5mM succinate, 2.5mM glutamate, 2.5mM malate, 1μM oligomycin, pH 7.2). After 1 min of incubation, absorbance at 520 nm was recorded using an Agilent Cary 100 UV-Vis spectrophotometer. Swelling rate was calculated as the decrease in absorbance over 1 minute of recording (using the SLOPE function of MS Excel). Two different mitochondrial preparations were used.

Co-immunoprecipitation

For the interaction between MITOSUR-Flag or MITOSUR^{K513A}-Flag and Mitok-V5, HeLa cells were transfected with the indicated plasmids. After 48 hours, cells were lysed in CoIP buffer (150mM NaCl, 1% Digitonin, 50mM Tris-Cl pH7.4, 1mM EGTA-Tris pH 7.4 and Complete EDTA-free protease inhibitor mixture). Lysates were centrifuged at 15000xg for 10 min, and supernatant was transferred into new tubes. One mg of proteins was precleared using a control agarose resin (Thermo Fisher Scientific) for 30 min at 4°C. Precleared proteins were incubated with monoclonal α-Flag-agarose-conjugated antibody (Sigma) for 3 hours at 4°C. After 3 washes (10') in CoIP buffer, 50 μl of Laemmli buffer 2X was added to the resin and heated for 5 min at 95°C. The precleared lysate (Input) and the immunoprecipitated (CoIP) fractions were separated and blotted as described above.

For the interaction between endogenous MITOK and MITOSUR, isolated mitochondria from mouse liver or HeLa cells were lysed in CoIP buffer and processed as indicated above. One mg of precleared proteins were incubated with 5 μg of anti-MITOK$_{N\text{-}term}$ (Sigma HPA010980) antibody for 3 hours. Protein A-Sepharose beads (GE Healthcare) were added for 1 hour and washed 3 times with CoIP buffer. 50 μl of Laemmli buffer 2X was added to the resin and heated for 5 min at 95°C. Results are representative of at least three independent transfections.

Analysis of OPA1 oligomers

HeLa cells were treated with 1 mM BMH (Thermo Fisher Scientific) for 30min at 37°C. After crosslinking reaction, cells were quenched and washed in PBS with 0.1% beta-mercaptoethanol (BME) twice. Cells were then lysed in RIPA buffer supplemented with BME and subjected to Western blot on NUPAGE Novex 3-8% Tris-acetate gradient gels (Thermo Fisher Scientific). Western blot provided in the figures is representative of three different crosslinking reactions.

Immunofluorescence and confocal imaging

HeLa cells were grown on 24 mm coverslips until 50% confluence. Cells were then washed with PBS, fixed in 4% formaldehyde for 10 minutes and quenched with 50 mM NH_4Cl in PBS. Cells were permeabilized for 10 minutes with 0.1% Triton X-100 in PBS and blocked in PBS containing 2% BSA for 1 hour. Cells were then incubated with primary antibodies (anti-mitoK, anti-HSP60) for 3 hours at room temperature and washed 3 times with 0.1% Triton X-100 in PBS. The appropriate isotype matched AlexaFluor-conjugated secondary antibodies (Thermo Fisher Scientific) were incubated for 1 hour at RT and coverslips were mounted with ProLong Gold Antifade reagent (Thermo Fisher Scientific). Alternatively,

cells were transfected with mitochondrial-targeted DsRed or mEmerald. 24 hours later, cells were fixed and mounted as described above. Images were acquired on a Leica TCS-SP5-II-RS-WLL equipped with a 100x, 1.4N.A. Plan-apochromat objective. AlexaFluor488 (or mEmerald) was excited by the 488 nm laser line and images were collected in the 495-535 nm range. AlexaFluor555 (or DsRed) was sequentially excited with the 543 nm laser line and signal was collected in the 555-600 nm range. Pixel size was set below 100 nm to meet the Nyquist criterion. For each image, a z-stack of the whole cell was acquired, with a step size of 130 nm. Images are presented as maximum projections of the whole stack using the Fiji image processing package based on ImageJ[45]. Images are representative of at least three independent transfections.

Analysis of mitochondrial morphology

HeLa cells were grown on 13 mm coverslips until 50% confluence and transfected with a plasmid encoding for a mitochondrial targeted mEmerald protein. After 36 hours, cells were washed 3 times with PBS and treated with and incubated in a KRB-based buffer containing 5.5mM 2-deoxyglucose. After 0, 15 or 60 minutes, cells were fixed and processed for confocal imaging as described above. Images (single planes) were than analyzed using a custom ImageJ script. Briefly, background and noise corrected images were thresholded and objects were counted with the “Analyze particles” function (using 0.2 μm^2 as lower cutoff). Objects were then classified as fragmented (circularity > 0.8 or length < 3μm), elongated (circularity < 0.2 or length > 6μm) or intermediate (other cases). Finally, for each cell, the area occupied by elongated, intermediate and fragmented mitochondria was normalized on the global mitochondrial area and expressed as percentage. At least 20 cells were analyzed per condition (more than 50 objects were counted in each cell) from 3 independent transfections.

Analysis of ROS production

HeLa cells were plated on 96-well black plates and grown until full confluency. Cells were then incubated for 45 minutes in a KRB-based buffer containing 5.5mM glucose supplemented with 0.02% Pluronic F127 and 5μM CM-H2DCFDA. Cells were washed twice with PBS and incubated in KRB-based buffer supplemented as indicated in the text. Fluorescence (excitation 485/10 nm, emission 530/30 nm, recorded from the bottom of the plate) was monitored on a Perkin Elmer Envision multi-mode plate reader operating at 37°C in well-scan mode. Blank was subtracted using two wells containing unstained cells. Fluorescence was recorded every 60 minutes over 16 hours. Total fluorescence was calculated for each well at each time point and the rate of fluorescence increase was calculated using the SLOPE function in MS Excel. At least 10 wells were analyzed from three independent experiments.

$[Ca^{2+}]_{mt}$ measurements

HeLa cells were grown on 13 mm round glass coverslips at 50% confluence and cotransfected with a low-affinity mitochondrial-targeted aequorin-based probe (mtAeqMut)[46] together with the indicated plasmid (the mock vector pcDNA3.1 was used as a control). 24/36 hours after transfection, cells were incubated with 5 μM coelenterazine for 1–2 hr in KRB (Krebs-Ringer modified buffer: 125 mM NaCl, 5 mM KCl, 1 mM Na_3PO_4, 1

mM $MgSO_4$, 5.5 mM glucose, 20 mM HEPES, pH 7.4) at 37°C supplemented with 1 mM $CaCl_2$, and then transferred to the perfusion chamber. All aequorin measurements were carried out in KRB. Agonists and other drugs were added to the same medium as specified in the text. The experiments were terminated by lysing cells with 100 μM digitonin in a hypotonic Ca^{2+}-rich solution (10 mM $CaCl_2$ in H_2O), thus discharging the remaining aequorin pool. The light signal was collected and calibrated into $[Ca^{2+}]$ values by an algorithm based on the Ca^{2+} response curve of aequorin at physiological conditions of pH, $[Mg^{2+}]$, and ionic strength, as previously described[46]. Alternatively, $[Ca^{2+}]$ measurements were carried out on a PerkinElmer Envision plate reader equipped with a two-injector unit. Cells were transfected as described above in 24-well plates and then replated into 96-well plates (1:5 dilution) the day before the experiment. After reconstitution with 5 μM coelenterazine, cells were placed in 70 μl of KRB and luminescence from each well was measured for 1 min. During the experiment, histamine was first injected at the desired concentration to activate calcium transients, and then a hypotonic, Ca^{2+}-rich, digitonin-containing solution was added to discharge the remaining aequorin pool. Output data were analyzed and calibrated with a custom made macro-enabled Excel workbook. All the results are expressed as mean ± s.d. and are representative of at least three independent transfections.

$\Delta\psi_m$ measurements

The measurement of mitochondrial membrane potential is based on the distribution of the mitochondrion-selective lipofilic cation dye TetraMethyl Rhodamine Methyl ester (Thermo Fisher Scientific). Cells were loaded with 20nM TMRM for 30 minutes at 37°C and then transferred to the imaging system. Images were acquired on a Zeiss Axiovert 200 microscope equipped with a 40x/1.3 N.A. PlanFluor objective. Excitation was performed with a Deltaram V high speed monochromator (Photon Technology International) equipped with a 75W Xenon Arc lamp. Images were captured with a high sensitivity Evolve 512 Delta EMCCD (Photometrics). The system is controlled by Metamorph 7.5 and was assembled by Crisel Instruments. TMRM excitation was performed at 560 nm and emission was collected through a 590–650 nm bandpass filter. Images were acquired every 5 seconds with a fixed 200 milliseconds exposure time. At the end of each experiment, 10μM CCCP was added to collapse $\Delta\psi_m$. After background correction, the fluorescence value after CCCP addition was subtracted for each cell. For the analysis of basal $\Delta\psi_m$, data are presented as raw fluorescence values in resting conditions. For the analysis of $\Delta\psi_m$ flashes, data are presented as time lapse of normalized fluorescence (F/F_0). Data were obtained from at least three independent preparations. All analyses were performed with the Fiji distribution of ImageJ.

Transmission electron microscopy

HeLa cells were grown in 24 well plates and fixed with 2.5% glutaraldehyde in 0.1M sodium cacodylate buffer pH 7.4 for 1 hour at 4°C, postfixed with a mixture of 1% osmium tetroxide and 1% potassium ferrocyanide in 0.1M sodium cacodylate buffer for 1 hour at 4° and incubated overnight in 0.25% uranyl acetate at 4°C. After three water washes, samples were dehydrated in a graded ethanol series and embedded in an epoxy resin (Sigma). Ultrathin sections (60-70 nm) were obtained with an Ultrotome V (LKB) ultramicrotome, counterstained with uranyl acetate and lead citrate and viewed with a Tecnai G2 (FEI)

transmission electron microscope operating at 100 kV. Images were captured with a Veleta (Olympus Soft Imaging System) digital camera. For structural quantification, the cristae width was measured from all mitochondria from 15 cells for each condition.

OCR measurements

OCR measurements were performed in intact HeLa cells using the XF24 Extracellular Flux Analyzer platform (Agilent) according to manufacturer's instructions. Cells were counted and plated on XF24 cell culture plates. The following day, growth medium was replaced with pre-warmed unbuffered DMEM (Sigma) and equilibrated for 1 hour at 37°C. Oligomycin (2μM), FCCP (0.4μM), rotenone (0.5μM) and antimycin A (0.5μM) were dissolved in assay medium and loaded on sensor cartridge ports. Oxygen consumption rate (OCR) was detected under basal conditions followed by the sequential addition of the indicated drugs[47].

Cell viability

HeLa cells of the indicated genotype were counted and plated in a 96-well plate. After 36 hours, growth medium was replaced with KRB containing the indicated H_2O_2 concentration. After 2 hours, PrestoBlue assay (Thermo Fisher Scientific) was performed according to manufacturer's instructions. Data are presented as % absorbance at 570 nm (600 nm as reference wavelength was used) relative to untreated cells. Three independent experiments with 16 replicates each have been performed.

Generation of Mitok-KO mice

Mitok-KO mice were generated by genOway (Lyon, France) on a C57BL/6N background. Two LoxP sites flanking exon 4 of murine *Mitok* gene were introduced by homologous recombination. The genotype was verified by PCR with the following primer:

Mitok-KO-FW1: GCACCTTGTCAGCACCATGACAACTC

Mitok-KO-FW2: GAGGGATCGCTGTGGAAGGCTGTAT

Mitok-KO-RV: GCGGACAAAGATTGTGTCACTGTTTGC

The KO allele yields an amplification product of 769 bp, while the wt allele generates a 278 bp fragment. All animal experiments were performed in accordance with the Italian law D. L.vo n_26/2014 and approved by local (O.P.B.A.) and national (Ministry of Health) committees (376-2015PR).

$^{86}Rb^+$ uptake measurements

After isolation, 200 mg of mitochondria from wt and Mitok-KO liver were resuspended in swelling buffer (100mM KCl, 20 mM HEPES, 1 mM $MgCl_2$, 2 mM Pi, 1 mM EGTA, 0.1% BSA, 5mM succinate, 2.5mM glutamate, 2.5mM malate, 1μM oligomycin, pH 7.2) containing trace amount (1-2 μCi) of $^{86}RbCl$. Where indicated, the buffer was supplemented with ATP (2 mM) and diazoxide (50 μM). After 1, 10, 20 and 30 minutes, mitochondria were rapidly centrifuged and washed. The amount of $^{86}Rb^+$ trapped within the organelle was estimated by scintillation counting and normalized on protein content. Rb^+ influx rate was

calculated as the relative increase in isotope content over time (using the SLOPE function of MS Excel). Results are expressed as mean ± s.d. of three independent experiments.

Ischemia reperfusion experiments

Adult (4 months-old) wt and Mitok-KO male mice were anaesthetized by means of an intraperitoneal injection of Zoletil 100 (30 mg/kg). Hearts were perfused with bicarbonate buffer gassed with 95% O_2–5% CO2 at 37 °C (pH 7.4) at a constant flux of 5 ml/min. Perfusion was performed in the nonrecirculating Langendorff mode, as previously described[48]. The perfusion buffer contained (in mM) 118.5 NaCl, 3.1 KCl, 1.18 KH_2PO_4, 25.0 $NaHCO_3$, 1.2 $MgCl_2$, 1.4 $CaCl_2$ and 5.6 glucose. Hearts were treated as follows (n≥5/group): after 10 min of normoxic stabilization, hearts were subjected to 40 min of global no-flow ischemia (I-40) followed by 15 min of reperfusion (R-15). Pharmacological preconditioning was carried out by perfusion in the presence diazoxide (30 μM) for 10 min, followed by the I/R protocol in the absence of diazoxide. After reperfusion hearts were quickly immersed into PBS containing 0.5% Triton X100 and homogenized for measurement of lactate dehydrogenase (LDH). For TTC staining, hearts were subjected to the I/R protocol and frozen at −20°C until used for quantification of myocardial infarct size. The hearts were cut into 5 transverse slices, incubated with 2,3,5-triphenyltetrazolium chloride (TTC, 1% w/v, pH 7.4) for 20 min at 37°C, and fixed overnight in 4% formaldehyde at 4C°.The slices were digitally photographed. The infarcted tissue stains a characteristic white color, whereas the viable tissue stains red. The infarct area was expressed as percentage of total area minus cavities and calculated using ImageJ. Please note that the whole heart is exposed to ischemia in Langendorff mode, and thus there is no need to normalize on area-at-risk.

Measurement of lactate dehydrogenase activity

To determine the amount of lactate dehydrogenase (LDH) released from the hearts exposed to I/R, coronary effluent was collected at 1 min intervals during the 15 min of reperfusion as previously described[49]. At the end of reperfusion hearts were homogenized for assessing the residual activity of LDH in the whole tissue. LDH activity was determined by means of a classic procedure. Since all values were normalized to heart weight, the amount of LDH released was expressed as % of total (i.e., effluent + homogenate) to rule out possible changes due to variations in heart size[50].

Statistical analysis of data

In bar graphs, data are presented as mean ± s.d. unless specified. For box plots, the boundary of the box closest to zero indicates the 25th percentile, the line within the box marks the median, and the boundary of the box farthest from zero indicates the 75th percentile. Whiskers (error bars) above and below the box indicate the 90th and 10th percentiles. Dots represent outlying points. Variance was calculated by one-way, two-way or three-way ANOVA as indicated in the legend, and multiple comparisons were assessed using the Holm-Sidak post hoc test. Where applicable, data points and exact p-values are indicated in source data tables. All analyses were performed with the SigmaPlot 12.0 (Systat Software Inc.) or Excel (Microsoft).

Europe PMC Funders Author Manuscripts

Extended Data

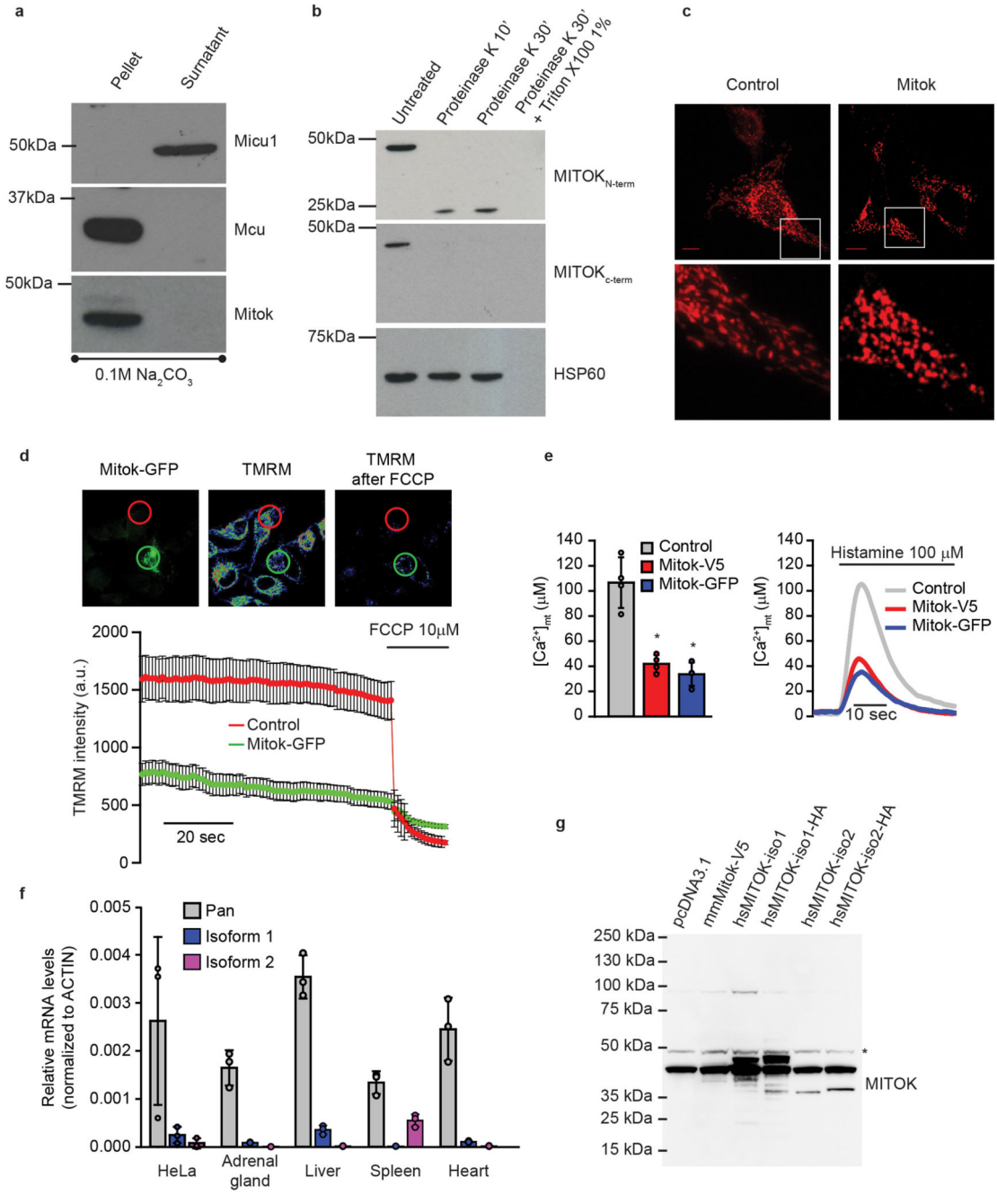

Extended data figure 1. Mitok overexpression causes mitochondrial dysfunction.

(a) Membrane (Pellet) and soluble (Surnatant) proteins were separated from isolated liver mitochondria using ice-cold 0.1M Na_2CO_3 (pH 11.5). Western blot is representative of three independent experiments. (b) Proteinase K protection assay in isolated liver mitochondria. Similar results were obtained in three independent reactions. (c) Mitochondrial morphology of control and Mitok-overexpressing HeLa cells (representative of five independent

Europe PMC Funders Author Manuscripts

experiments; scale bar is 10 μm). (d) Representative images and average ± s.d. traces of control and Mitok-GFP expressing HeLa cells loaded with TMRM. n = 9 biologically replicates from three independent experiments. (e) $[Ca^{2+}]_{mt}$ measurements (mean ± s.d.) in intact HeLa expressing the indicated constructs; n = 4 biological replicates (representative of three independent experiments), * $p < 0.001$ using one-way ANOVA with Holm-Sidak correction. (f) qPCR analyses of transcripts from HeLa cells or the indicated human tissues using specific (isoform 1 and isoform 2) or non-specific (pan) primer pairs for MITOK. Data were normalized to ACTIN and expressed as mean ± s.d. For HeLa cells, n=3 biologically independent samples. For human tissues, n=3 technical replicates. (g) Protein expression of MITOK isoforms in HeLa cells transfected with the indicated constructs. Asterisk indicates a non-specific band. Image is representative of two independent experiments.

Europe PMC Funders Author Manuscripts

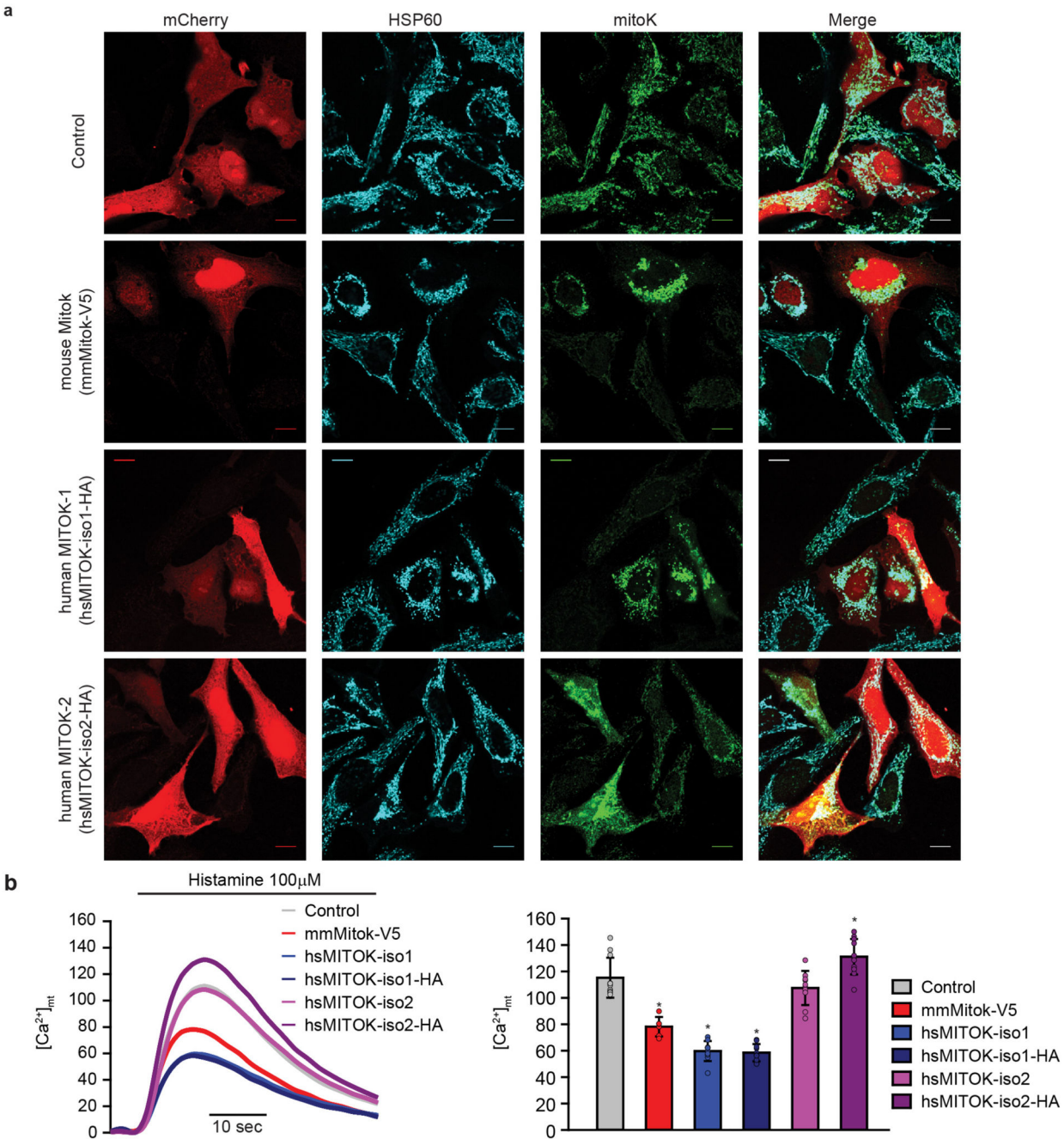

Extended data figure 2. Localization and function of human MITOK isoforms.

(a) Immunolocalization of MITOK (green) and the mitochondrial marker HSP60 (cyan) in HeLa cells transfected with the indicated constructs (images are representative of two independent experiments; scale bar is 10 μm). (b) $[Ca^{2+}]_{mt}$ measurements (mean ± s.d.) in intact HeLa expressing the indicated constructs; n ≥ 6 independent samples, * $p < 0.001$ using one-way ANOVA with Holm-Sidak correction.

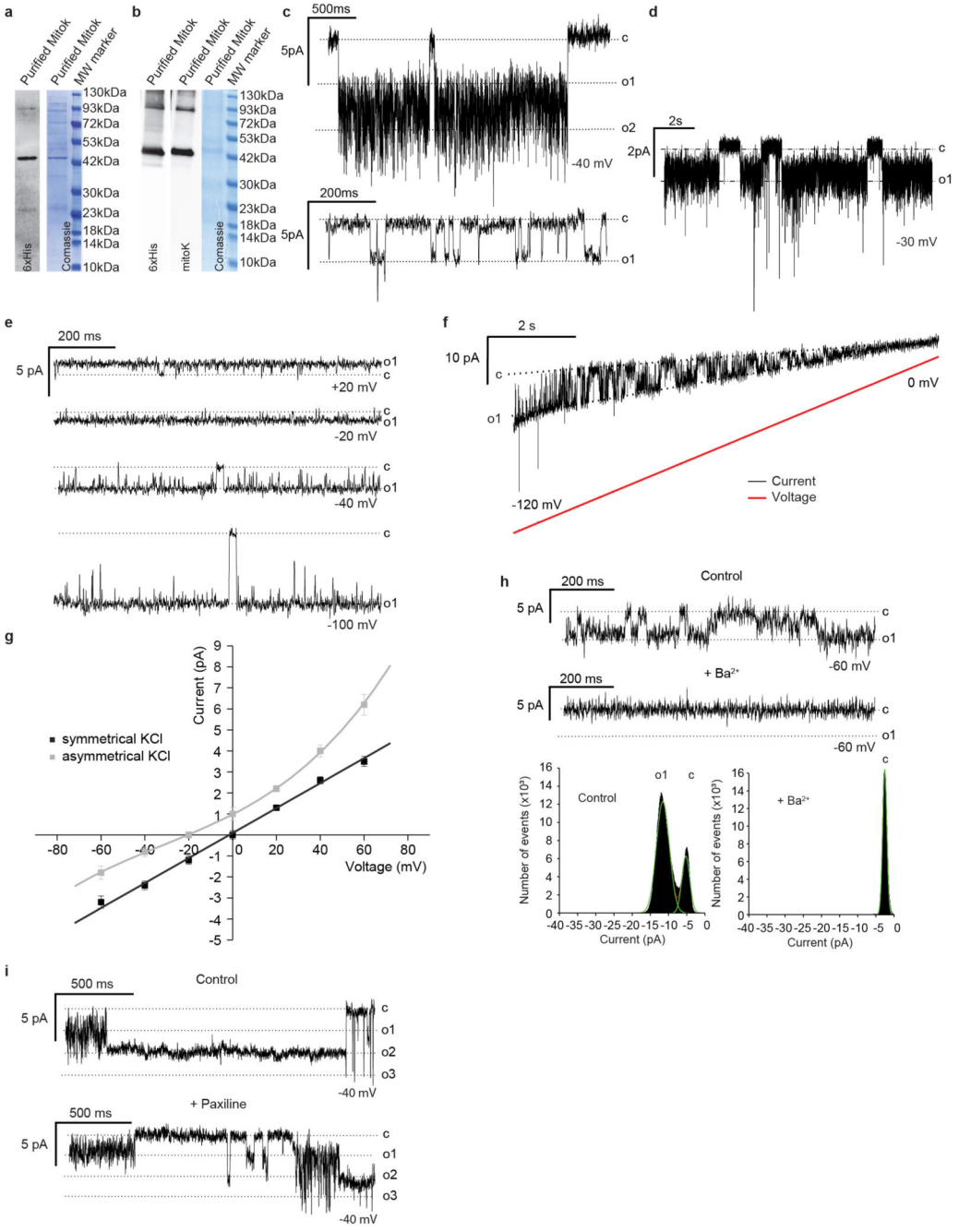

Extended data figure 3. Mitok is a cation channel.

(a-b) (a) Western blots and Coomassie of Mitok expressed and purified from E.coli (a) or WGL (b), representative of three independent experiments. (c) Current traces showing two channels gating together resulting in flickering activity (upper panel) or normal single channel activity (lower panel). The two traces were recorded in the same experiment, performed in 100 mM Kgluconate medium and representative of five independent experiments. (d) Current trace showing burst like activity and cooperative transition between dual- or multi-states of two channels. Recording was performed in 100 mM Kgluconate

Europe PMC Funders Author Manuscripts

medium. Similar activity was present in more than six recordings. (e) Representative traces of Mitok channel activity at the indicated voltages. Similar results were obtained in three independent experiments. (f) Voltage ramp (from -120 mV to 0 mV) of Mitok recorded in 100 mM Kgluconate symmetrical medium (n=3 independent experiments). (g) Single-channel i-V curves under symmetric (black) and asymmetric (grey) ionic conditions (mean value ± s.d., n = 50 from 3-4 different experiments for each point). Fitting revealed an E_{rev} = -21.6 ± 1 mV (n=4 independent experiments). (h) Representative traces (upper panels) and amplitude histograms (lower panels) before and after the addition of 2 mM Ba^{2+} (n=4 independent experiments) in 100 mM KCl medium. (i) Representative traces (upper panels) and amplitude histograms (lower panels) of Mitok activity before (Control) and after paxilline (40 μM) addition (n=4 independent experiments).

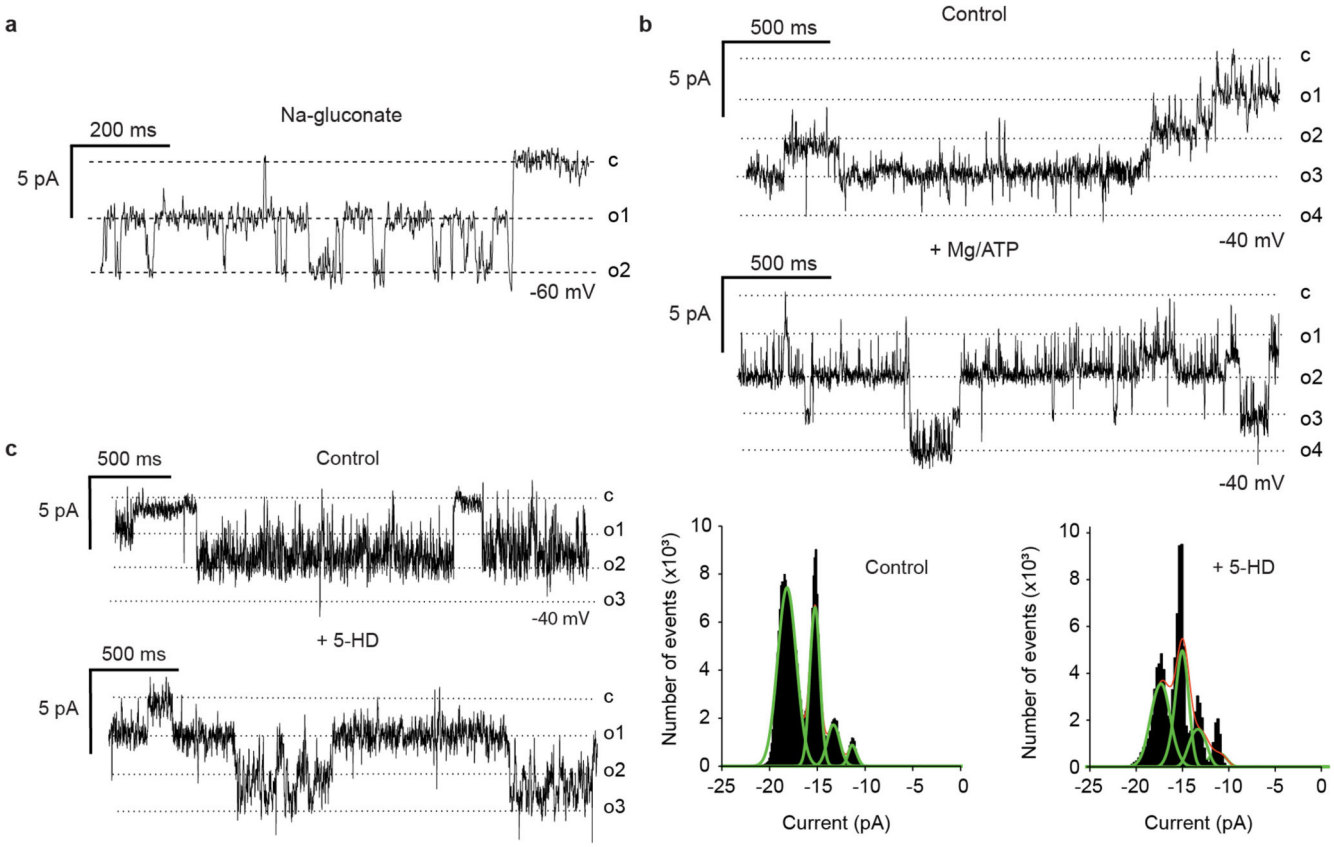

Extended data figure 4. Mitok alone is insensitive to ATP.

(a) Activity of Mitok in 100 mM Na-gluconate (n=5 independent experiments). (b) Current traces of Mitok channel activity obtained from 60 s recordings (in 100 mM K-gluconate) before (upper panel) and after (lower panel) addition of 2 mM Mg/ATP (representative of 8 independent experiments). Voltages of cis side are reported. (c) Representative traces (left panels) and amplitude histograms (right panels) of Mitok activity before (Control) and after 5-HD (100 μM) addition (n=5 independent experiments).

Europe PMC Funders Author Manuscripts

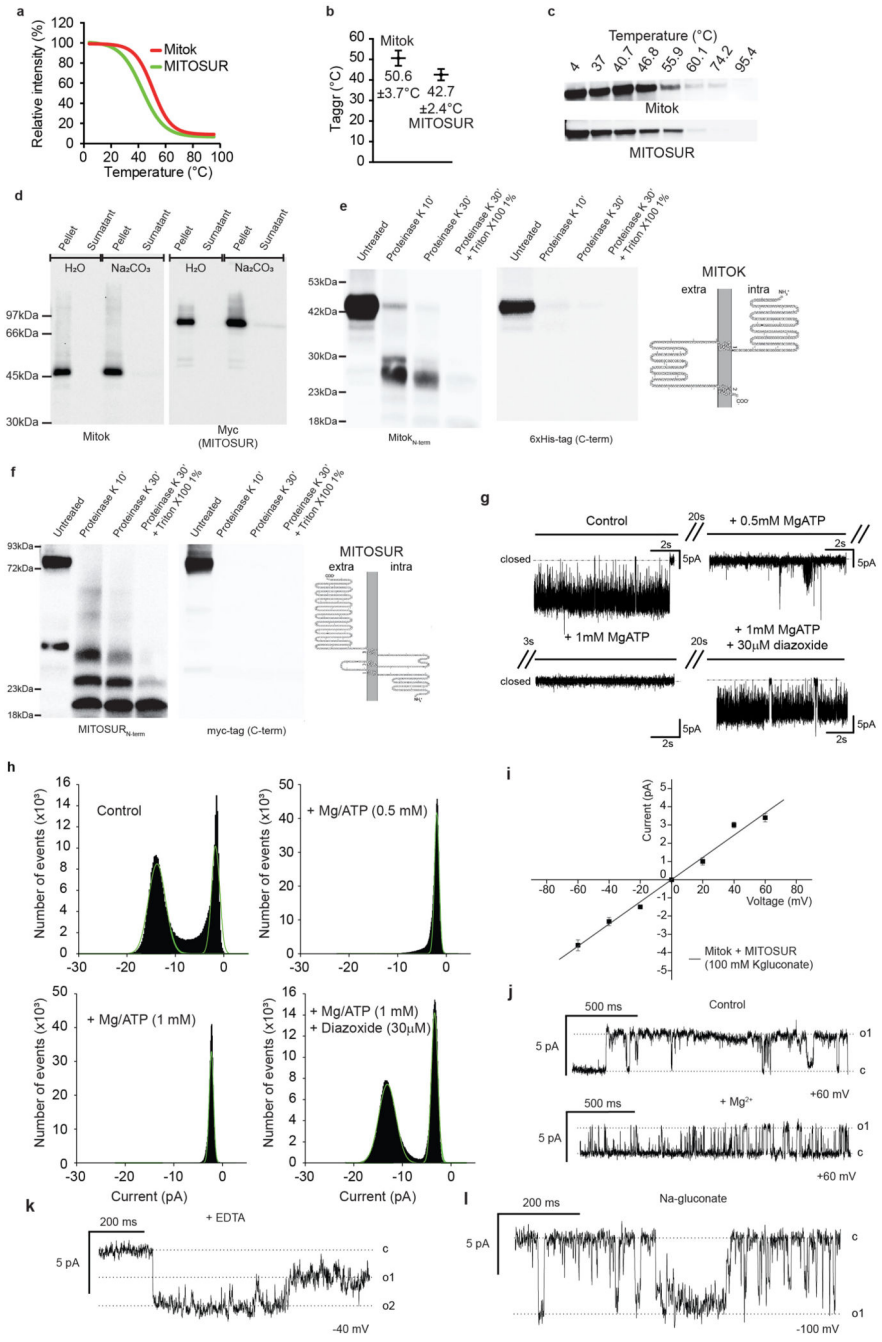

Extended data figure 5. Biophysical characterization of recombinant Mitok and MITOSUR.

(a-c) Thermal shift assay analysis of Mitok and MITOSUR: average curves (a), graphs of Taggr (b, expressed as mean ± s.d.) and Western blot (c), representative of 4 independent experiments. (d) Membrane extraction and Western blot (representative of two independent experiments) of *in vitro* co-expressed Mitok and MITOSUR incorporated into liposomes. (e-f) Membrane topology assessed by proteinase K protection assay in reconstituted liposomes and probed for Mitok (e) and MITOSUR (f). (g) The same experiment shown in Figure 2a is here represented with a different time scale. (h) Amplitude histograms of channel activity

before (Control) and after first addition of 500 μM Mg/ATP, second addition of 500 μM Mg/ATP, and third addition of 30 μM diazoxide. Similar results were obtained with 4 independent preparations. (i) Single channel current (i)-voltage (V) relationship of Mitok and MITOSUR. Linear fitting revealed a chord conductance of 63±3 pS (n=4 independent experiments). (j) Activity in the absence (Control, left panel) and presence of 1 mM Mg^{2+} (right panel) in 100 mM Kgluconate medium (n=3 independent experiments). (k) Activity of Mitok + MITOSUR in 100 mM K-gluconate, 5 mM EDTA, 10 mM Hepes, pH 7.4 (n=3 independent experiments). (l) Mitok + MITOSUR channel activity in 100 mM Na-gluconate medium (n=4 independent experiments).

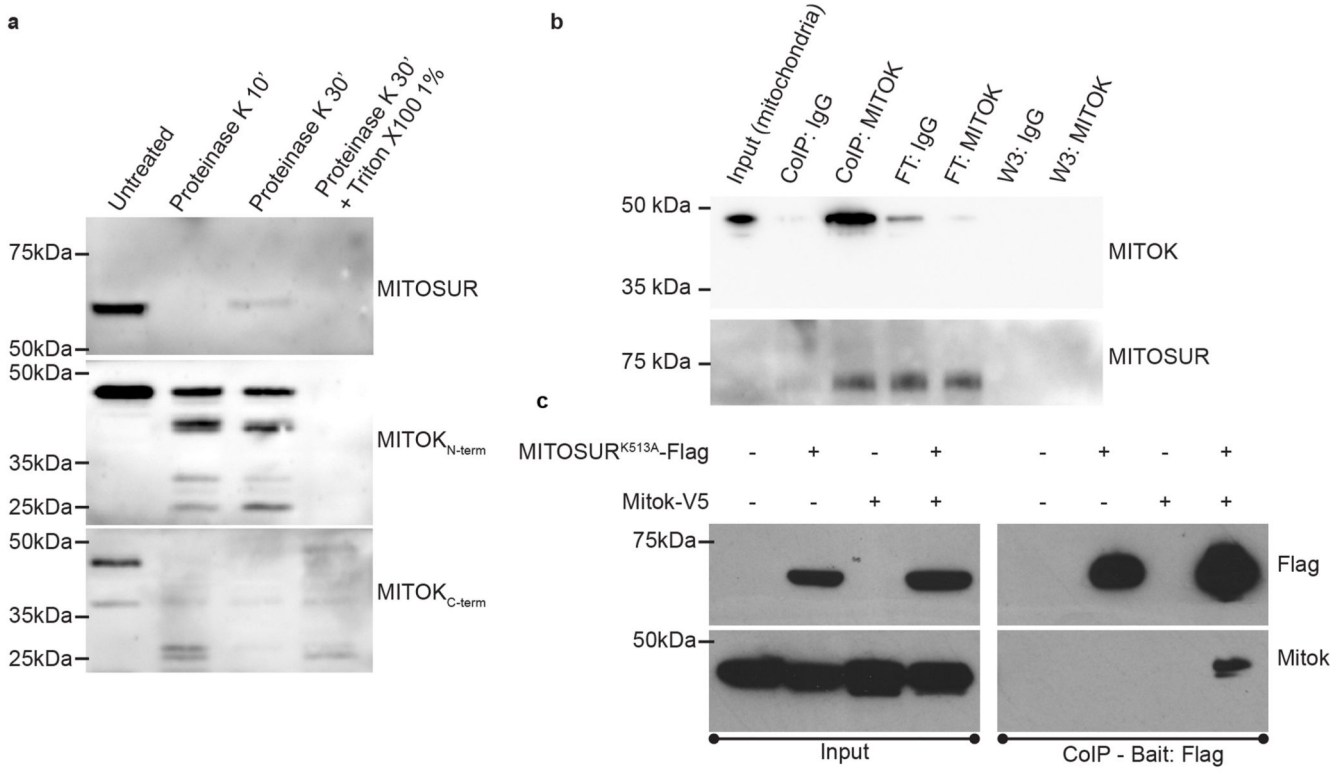

Extended data figure 6. MITOK and MITOSUR interact in situ.

(a) Proteinase K protection assay in isolated HeLa mitochondria. Similar results were obtained in two independent reactions. (b) Co-immunoprecipitation of endogenous Mitok using mitochondria isolated from HeLa cells. FT: flow-through fraction; W3: third (last) CoIP wash. Representative of two independent experiments (c) Co-immunoprecipitation between overexpressed Mitok and mutant $MITOSUR^{K513A}$. Representative of two independent experiments.

Europe PMC Funders Author Manuscripts

Europe PMC Funders Author Manuscripts

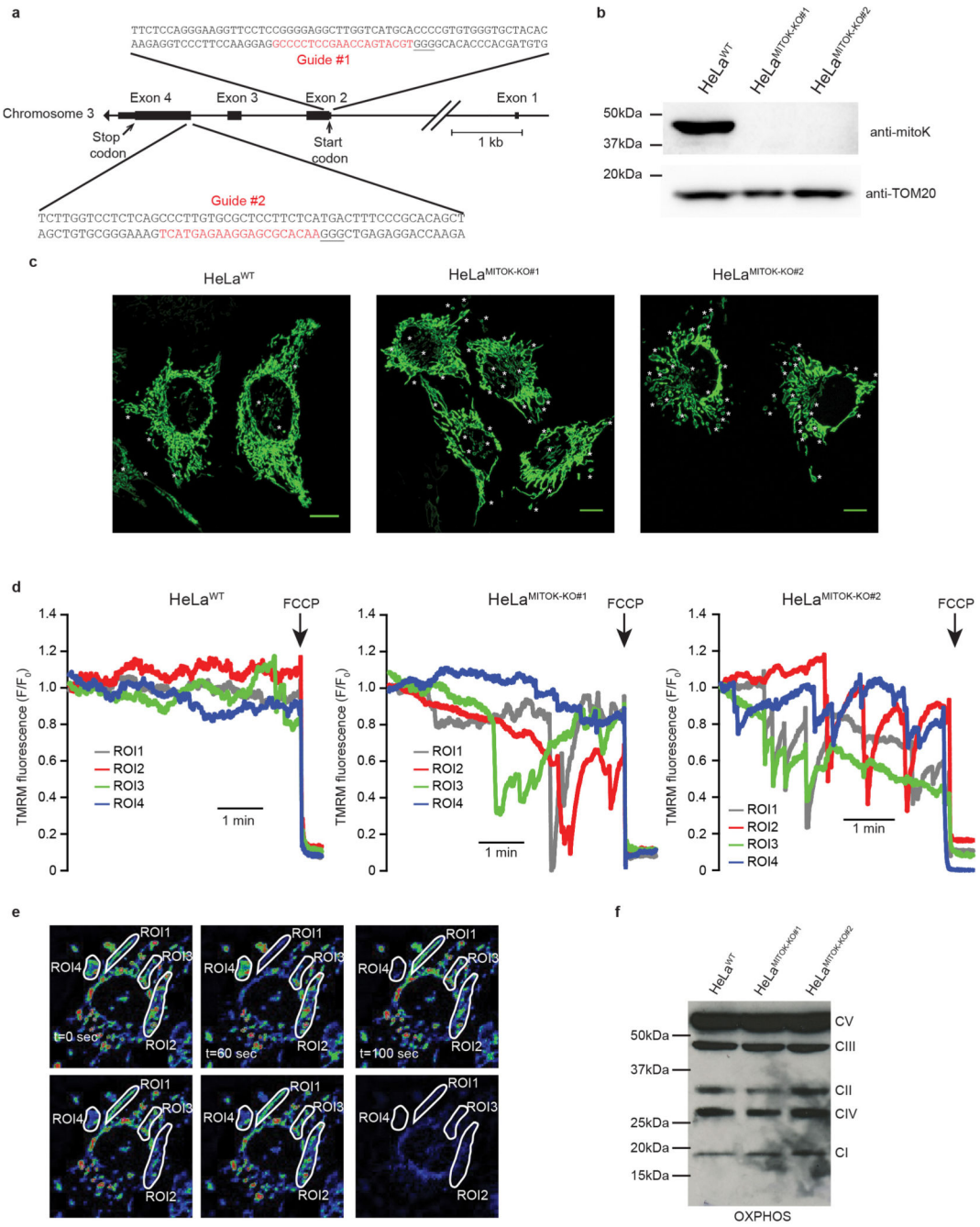

Extended data figure 7. Genetic ablation of MITOK in HeLa cells.

(a) Schematic representation of the human *MITOK* gene. The expanded regions were used to design Cas9 guides (highlighted in red). (b) Western blot of wild type and MITOK-KO HeLa cell lines (representative of three independent experiments). (c) Mitochondrial morphology in wild type and MITOK-KO HeLa cells. (scale bar is 10 μm). Asterisks are located near doughnut-shaped mitochondria. Similar results were obtained in five independent experiments. (d-e) $\Delta\psi_m$ measurements in control and MITOK-KO cells. Cells were loaded with TMRM and normalized fluorescence in different regions was monitored

through time. (d) Representative traces of single mitochondria. (e) Pseudo-colored representative images of a HeLa$^{MITOK-KO#1}$ cell loaded with TMRM at the indicated time points. Similar results were obtained in four independent experiments. (f) Western blot in HeLa cells of the indicated genotype. Representative of two independent experiments.

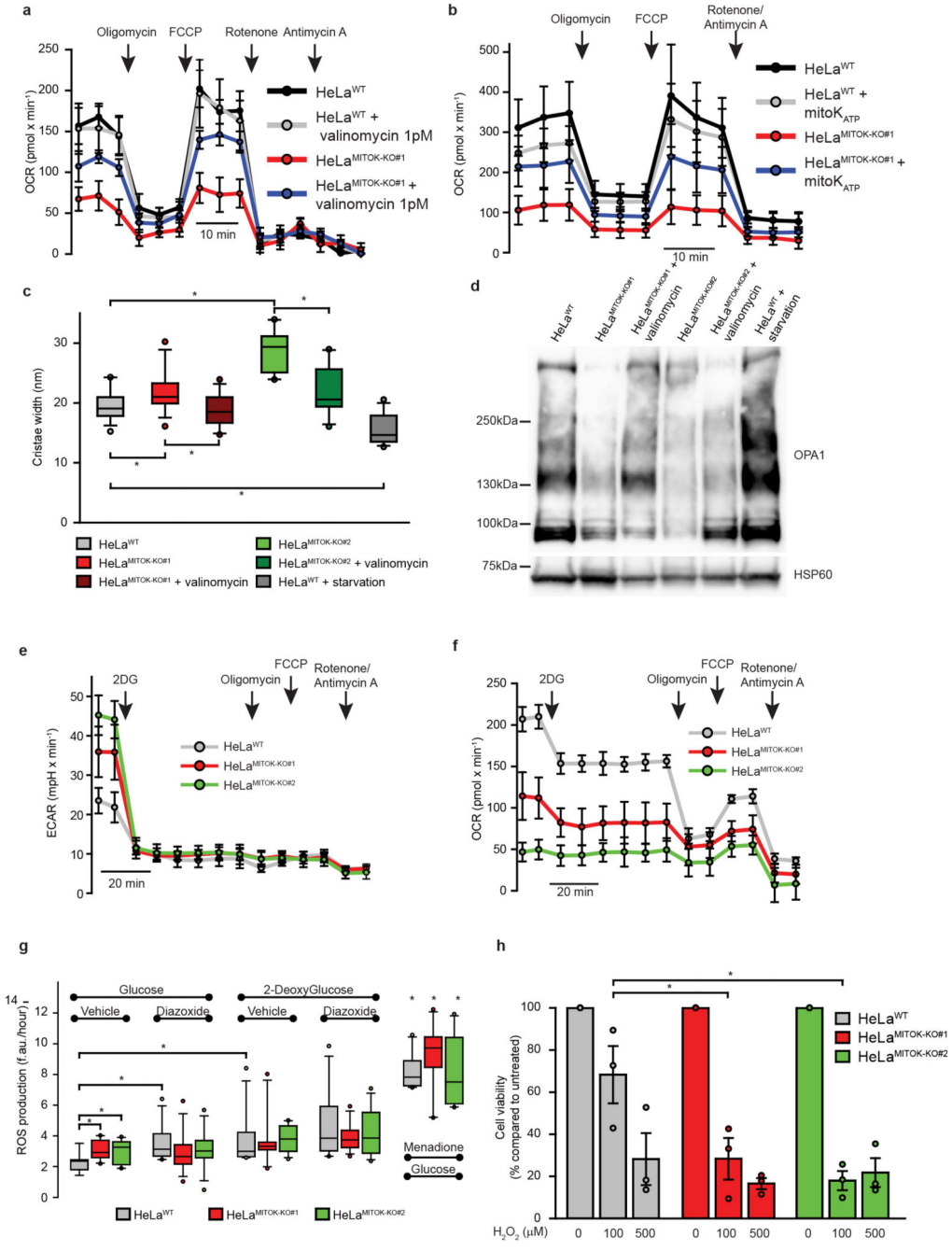

Extended data figure 8. Loss of MITOK causes mitochondrial dysfunction.

(a) OCR measurements in wt and MITOK-KO HeLa cells treated with either vehicle or 1pM valinomycin for 1 hour. Representative of three independent experiments (b) OCR

measurements in wt and MITOK-KO HeLa cells transfected with control or mitoK_{ATP} expressing (MITOSUR-P2A-Mitok) plasmids. Representative of three independent experiments. (c) Maximal cristae width in the indicated genotype. n ≥ 12 individual cells (approximately 20 cristae per cell were measured) from two independent preparations, * p ≤ 0.013 using two-way ANOVA with Holm-Sidak correction. (d) OPA1 crosslinking (using 1mM BMH) in wt and MITOK-KO cells. Similar results were obtained in three independent experiments. (e-f) ECAR (e) and OCR (f) measurements in intact cells of the indicated genotype. n = 5 biological replicates, representative of two independent experiments. (g) ROS production during energy stress. Cells were incubated in 5.5 mM of either glucose or 2-deoxyglucose in the presence or absence of 30 μM diazoxide and fluorescence were monitored for 16 hours. Box plots indicate the rate of ROS production over this time frame. n ≥ 10, * p < 0.05 using three-way ANOVA with Holm-Sidak correction. (h) Cell death analysis in HeLa cells treated with 0, 100 or 500 μM H_2O_2. Data were normalized to the untreated condition and expressed as mean ± s.d. n = 3 independent experiments, * p < 0.003 using two-way ANOVA with Holm-Sidak correction.

Supplementary Material

Refer to Web version on PubMed Central for supplementary material.

Acknowledgments

The authors are grateful to Paolo Bernardi, Valeria Petronilli, Tullio Pozzan, Luca Scorrano and Mario Zoratti for helpful discussion, to Federico Caicci and Francesco Boldrin for electron microscopy, to Aldo Montagna for immunofluorescence, to Luca Carraretto for help with expression of mitoK in *E.coli*, to Laura Cendron for the help with thermal shift assay and to Maria Ruzzene and Luca Cesaro for the help with radioactive assay. This work was supported by grants from the University of Padova (Assegno junior 2015 and SID 2016 to D.D.S., STARS@UNIPD WiC grant 2017 to R.R. and UNIPD funds for research equipment 2015), the Italian Ministry of Education, University and Research (FIRB to R.R. PRIN no. 2015795S5W to I.S.), the European Union (ERC mitoCalcium, no. 294777 to R.R.), NIH (Grant #1P01AG025532-01A1 to R.R.), the Italian Association for Cancer Research (AIRC IG18633 to R.R. and IG20286 to I.S.), and Telethon-Italy (GGP16029 to R.R.).

Data availability

Source data for Figures 3d-e, 4a-d, 4f, 5a-b, 5d and Extended Data Figures 1d-f, 2b, 3g, 5a-b, 5i, 7d, 8a-c and 8f-h have been provided in Source Data Tables. All other data supporting the findings of this study are available from the corresponding authors on request.

References

1. Ashcroft FM, Harrison DE, Ashcroft SJ. Glucose induces closure of single potassium channels in isolated rat pancreatic beta-cells. Nature. 1984; 312:446–8. [PubMed: 6095103]
2. Ashcroft FM, Rorsman P. K(ATP) channels and islet hormone secretion: new insights and controversies. Nat Rev Endocrinol. 2013; 9:660–9. [PubMed: 24042324]
3. Nichols CG. KATP channels as molecular sensors of cellular metabolism. Nature. 2006; 440:470–6. [PubMed: 16554807]
4. Inoue I, Nagase H, Kishi K, Higuti T. ATP-sensitive K+ channel in the mitochondrial inner membrane. Nature. 1991; 352:244–247. [PubMed: 1857420]
5. Paucek P, et al. Reconstitution and partial purification of the glibenclamide-sensitive, ATP-dependent K+ channel from rat liver and beef heart mitochondria. J Biol Chem. 1992; 267:26062–26069. [PubMed: 1464617]

6. Garlid KD, Halestrap AP. The mitochondrial K(ATP) channel--fact or fiction? J Mol Cell Cardiol. 2012; 52:578–83. [PubMed: 22240339]
7. Augustynek BB, Kunz WS, Szewczyk A. Guide to the Pharmacology of Mitochondrial Potassium Channels. Handbook of experimental pharmacology. 2016; 240:103–127.
8. Nessa A, Rahman SA, Hussain K. Hyperinsulinemic Hypoglycemia – The Molecular Mechanisms. Front Endocrinol (Lausanne). 2016; 7:29. [PubMed: 27065949]
9. Garlid KD, et al. Cardioprotective effect of diazoxide and its interaction with mitochondrial ATP-sensitive K+ channels. Possible mechanism of cardioprotection. Circ Res. 1997; 81:1072–1082. [PubMed: 9400389]
10. O'Rourke B. Evidence for mitochondrial K+ channels and their role in cardioprotection. Circ Res. 2004; 94:420–32. [PubMed: 15001541]
11. Sato T, Sasaki N, Seharaseyon J, O'Rourke B, Marban E. Selective Pharmacological Agents Implicate Mitochondrial but Not Sarcolemmal KATP Channels in Ischemic Cardioprotection. Circulation. 2000; 101:2418–2423. [PubMed: 10821820]
12. Wojtovich AP, et al. Kir6.2 is not the mitochondrial KATP channel but is required for cardioprotection by ischemic preconditioning. Am J Physiol Heart Circ Physiol. 2013; 304:H1439–45. [PubMed: 23585131]
13. Szabo I, Zoratti M. Mitochondrial channels: ion fluxes and more. Physiol Rev. 2014; 94:519–608. [PubMed: 24692355]
14. Smith CO, Nehrke K, Brookes PS. The Slo(w) path to identifying the mitochondrial channels responsible for ischemic protection. Biochem J. 2017; 474:2067–2094. [PubMed: 28600454]
15. Calvo SE, Clauser KR, Mootha VK. MitoCarta2.0: an updated inventory of mammalian mitochondrial proteins. Nucleic Acids Res. 2015; doi: 10.1093/nar/gkv1003
16. The GTEx Consortium. et al. The Genotype-Tissue Expression (GTEx) pilot analysis: Multitissue gene regulation in humans. Science (80-.). 2015; 348:648–660.
17. Dahlem YA, et al. The human mitochondrial KATP channel is modulated by calcium and nitric oxide: a patch-clamp approach. Biochim Biophys Acta - Bioenerg. 2004; 1656:46–56.
18. Bednarczyk P, et al. Quinine inhibits mitochondrial ATP-regulated potassium channel from bovine heart. J Membr Biol. 2004; 199:63–72. [PubMed: 15383917]
19. Choma K, et al. Single channel studies of the ATP-regulated potassium channel in brain mitochondria. J Bioenerg Biomembr. 2009; 41:323–334. [PubMed: 19821034]
20. Cang C, Aranda K, Seo Y, Gasnier B, Ren D. TMEM175 Is an Organelle K+ Channel Regulating Lysosomal Function. Cell. 2015; 162:1101–1112. [PubMed: 26317472]
21. Schaedler TA, et al. Structures and functions of mitochondrial ABC transporters. Biochem Soc Trans. 2015; 43
22. Ardehali H, Chen Z, Ko Y, Mejía-Alvarez R, Marbán E. Multiprotein complex containing succinate dehydrogenase confers mitochondrial ATP-sensitive K+ channel activity. Proc Natl Acad Sci U S A. 2004; 101:11880–5. [PubMed: 15284438]
23. Lee S-Y, et al. Architecture Mapping of the Inner Mitochondrial Membrane Proteome by Chemical Tools in Live Cells. J Am Chem Soc. 2017; 139:3651–3662. [PubMed: 28156110]
24. Bernardi P. Mitochondrial transport of cations: channels, exchangers, and permeability transition. Physiol Rev. 1999; 79:1127–1155. [PubMed: 10508231]
25. Liu X, Hajnóczky G. Altered fusion dynamics underlie unique morphological changes in mitochondria during hypoxia–reoxygenation stress. Cell Death Differ. 2011; 18:1561–1572. [PubMed: 21372848]
26. Duchen MR, Leyssens A, Crompton M. Transient mitochondrial depolarizations reflect focal sarcoplasmic reticular calcium release in single rat cardiomyocytes. J Cell Biol. 1988; 142:975–88.
27. Schwarzländer M, et al. Pulsing of membrane potential in individual mitochondria: a stress-induced mechanism to regulate respiratory bioenergetics in Arabidopsis. Plant Cell. 2012; 24:1188–201. [PubMed: 22395486]
28. Wang W, et al. Superoxide Flashes in Single Mitochondria. Cell. 2008; 134:279–290. [PubMed: 18662543]

29. Rosselin M, Santo-Domingo J, Bermont F, Giacomello M, Demaurex N. L-OPA1 regulates mitoflash biogenesis independently from membrane fusion. EMBO Rep. 2017; 18:451–463. [PubMed: 28174208]
30. Leanza L, et al. Direct Pharmacological Targeting of a Mitochondrial Ion Channel Selectively Kills Tumor Cells In Vivo. Cancer Cell. 2017; 31:516–531.e10. [PubMed: 28399409]
31. Garlid KD, Paucek P. The mitochondrial potassium cycle. IUBMB Life. 2009; 52:153–8.
32. Patten DA, et al. OPA1-dependent cristae modulation is essential for cellular adaptation to metabolic demand. EMBO J. 2014; 33:2676–91. [PubMed: 25298396]
33. Costa ADT, Garlid KD. Intramitochondrial signaling: interactions among mitoKATP, PKCepsilon, ROS, and MPT. Am J Physiol Heart Circ Physiol. 2008; 295:874–82.
34. Varanita T, et al. The Opa1-Dependent Mitochondrial Cristae Remodeling Pathway Controls Atrophic, Apoptotic, and Ischemic Tissue Damage. Cell Metab. 2015; 21:834–844. [PubMed: 26039448]
35. Liu Y, Sato T, O'Rourke B, Marban E. Mitochondrial ATP-Dependent Potassium Channels : Novel Effectors of Cardioprotection? Circulation. 1998; 97:2463–2469. [PubMed: 9641699]
36. Walters AM, Porter GA, Brookes PS. Mitochondria as a drug target in ischemic heart disease and cardiomyopathy. Circ Res. 2012; 111:1222–36. [PubMed: 23065345]
37. Foster DB, et al. Mitochondrial ROMK channel is a molecular component of mitoKATP. Circ Res. 2012; 111:446–454. [PubMed: 22811560]
38. Ye J, et al. Primer-BLAST: A tool to design target-specific primers for polymerase chain reaction. BMC Bioinformatics. 2012; 13:134. [PubMed: 22708584]
39. Carraretto L, et al. A Thylakoid-Located Two-Pore K^+ Channel Controls Photosynthetic Light Utilization in Plants. Science (80-.). 2013; 342:114–118.
40. Teardo E, et al. Physiological Characterization of a Plant Mitochondrial Calcium Uniporter in Vitro and in Vivo. Plant Physiol. 2017; 173:1355–1370. [PubMed: 28031475]
41. Ashok Y, Nanekar R, Jaakola V-P. Defining thermostability of membrane proteins by western blotting. Protein Eng Des Sel. 2015; 28:539–42. [PubMed: 26384510]
42. Hsu PD, et al. DNA targeting specificity of RNA-guided Cas9 nucleases. Nat Biotechnol. 2013; 31:827–832. [PubMed: 23873081]
43. Sanjana NE, Shalem O, Zhang F. Improved vectors and genome-wide libraries for CRISPR screening. Nat Methods. 2014; 11:783–784. [PubMed: 25075903]
44. Frezza C, Cipolat S, Scorrano L. Organelle isolation: functional mitochondria from mouse liver, muscle and cultured fibroblasts. Nat Protoc. 2007; 2:287–295. [PubMed: 17406588]
45. Schindelin J, et al. Fiji: an open-source platform for biological-image analysis. Nat Methods. 2012; 9:676–682. [PubMed: 22743772]
46. Granatiero V, Patron M, Tosatto A, Merli G, Rizzuto R. Using targeted variants of aequorin to measure Ca2+ levels in intracellular organelles. Cold Spring Harb Protoc. 2014; 2014:86–93. [PubMed: 24371314]
47. Nicholls DG, et al. Bioenergetic profile experiment using C2C12 myoblast cells. J Vis Exp. 2010; :3–7. DOI: 10.3791/2511
48. Carpi A, et al. The cardioprotective effects elicited by p66Shc ablation demonstrate the crucial role of mitochondrial ROS formation in ischemia/reperfusion injury. Biochim Biophys Acta - Bioenerg. 2009; 1787:774–780.
49. Di Lisa F, Menabo R, Canton M, Barile M, Bernardi P. Opening of the mitochondrial permeability transition pore causes depletion of mitochondrial and cytosolic NAD+ and is a causative event in the death of myocytes in postischemic reperfusion of the heart. J Biol Chem. 2001; 276:2571–2575. [PubMed: 11073947]
50. Schluter KD, Schwartz P, Siegmund B, Piper HM. Prevention of the oxygen paradox in hypoxic-reoxygenated hearts. Am J Physiol Circ Physiol. 1991; 261:H416–H423.

Europe PMC Funders Author Manuscripts

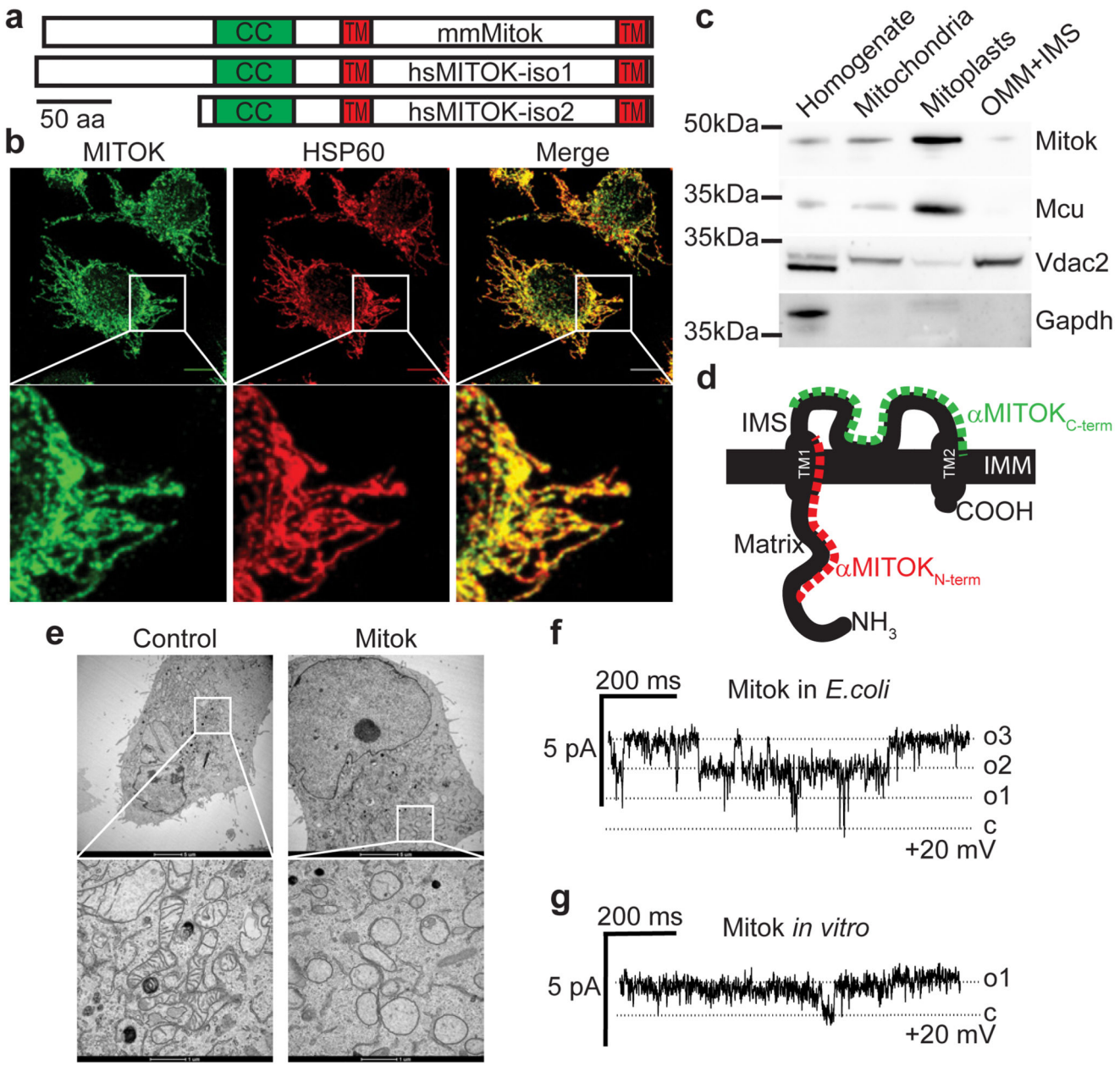

Figure 1. Biochemical and functional characterization of MITOK.

(a) Representation of human and murine MITOK proteins. Transmembrane (TM) and coiled-coil (CC) domains are indicated. (b) Immunolocalization of MITOK (green) and the mitochondrial marker HSP60 (red) (representative of four independent experiments; scale bar is 10 μm). (c) Subcellular fractionation of mouse liver (replicated twice). (d) Representation of MITOK membrane topology. (e) TEM images of control and Mitok-overexpressing HeLa cells (replicated three times). (f-g) Representative current traces with Mitok purified from E.coli (f, n=5 biological replicates from two independent preparations) or expressed in vitro (g, n=23 biological replicates from 10 independent preparations).

Europe PMC Funders Author Manuscripts

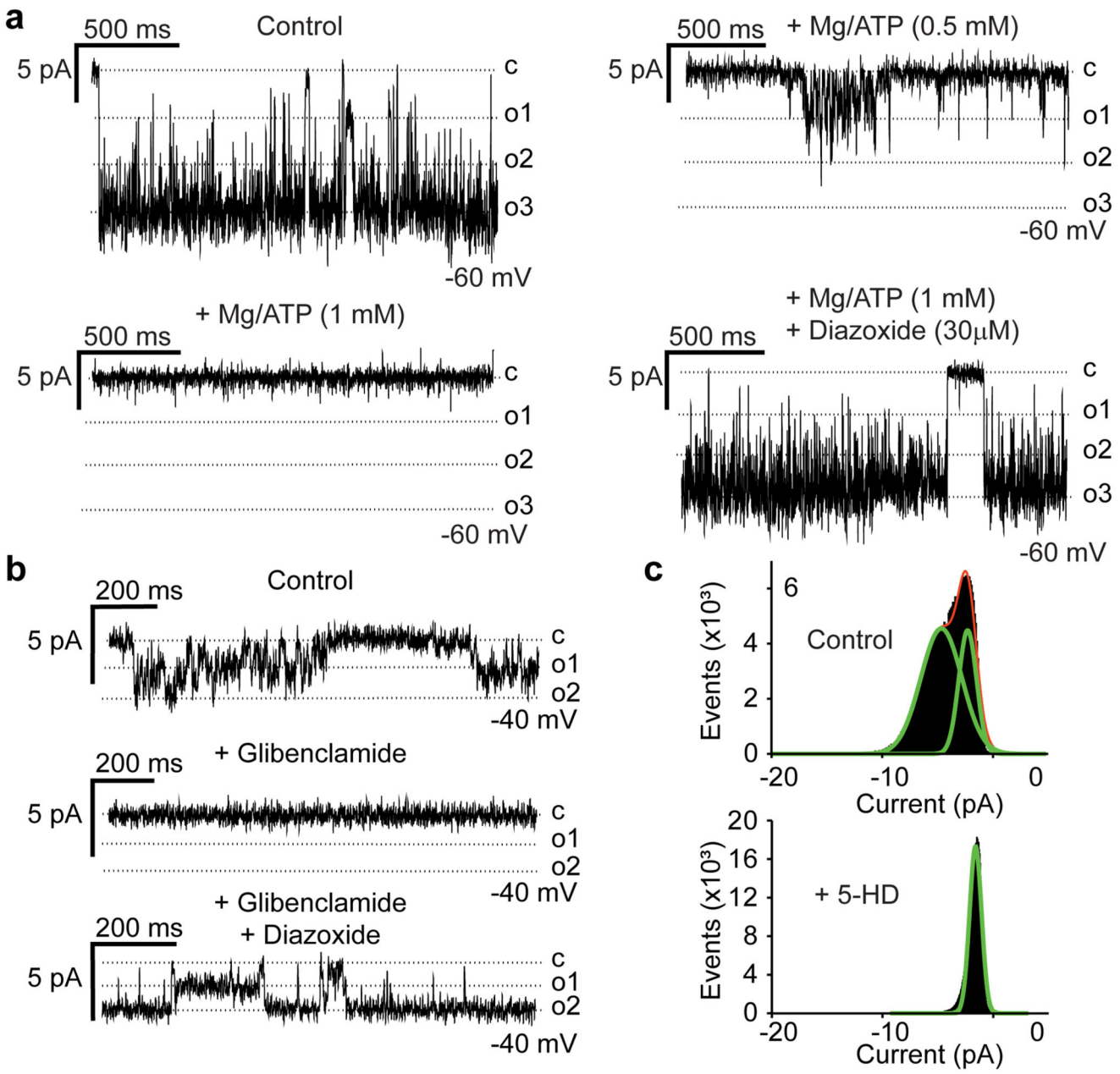

Figure 2. Electrophysiological characterization of recombinant Mitok co-expressed with MITOSUR.

(a) Current traces before (Control) and after first addition of 500 μM Mg/ATP, second addition of 500 μM Mg/ATP, and third addition of 30 μM diazoxide. All traces were obtained from the same experiment, representative of 4 independent experiments. (b) Current recordings before and after addition of 30 μM glibenclamide. The channel was re-activated by subsequent addition of 100 μM diazoxide (n= 4 for inhibition by glibenclamide, n=2 for reactivation by diazoxide). (c) Representative histograms before (upper panel) and after (lower panel) addition of 5-HD (100 μM, n = 5 independent experiments).

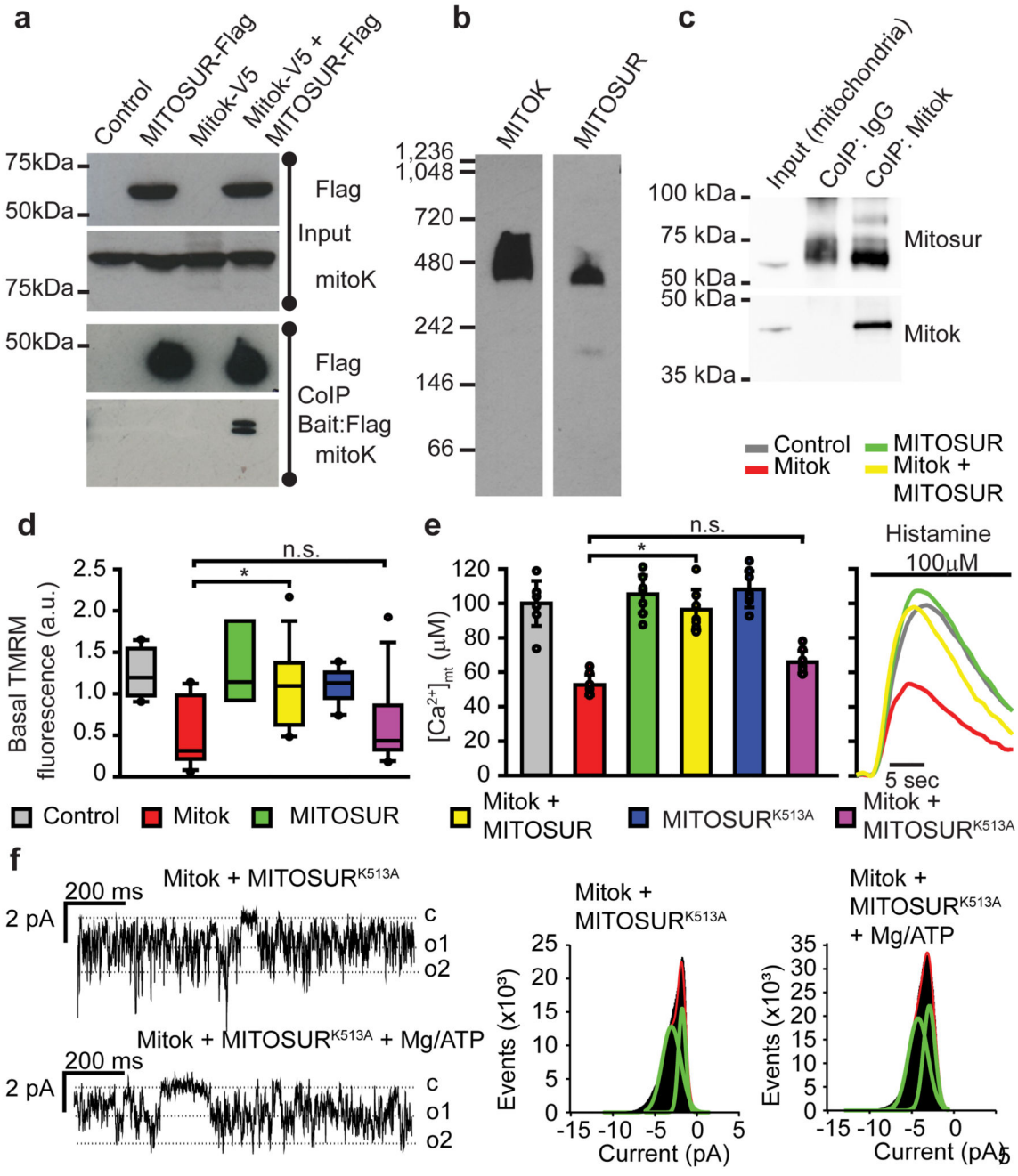

Figure 3. MITOK and MITOSUR form the mitoK$_{ATP}$ in situ.

(a) Co-immunoprecipitation between overexpressed Mitok and MITOSUR (representative of three independent experiments). (b) Blue-native PAGE of digitonin-permeabilized mitochondria (representative of two independent experiments). (c) Co-immunoprecipitation of endogenous Mitok using liver mitochondria (representative of two independent experiments). (d) $\Delta\psi_m$ measurements in HeLa cells transfected with the indicated constructs. n ≥ 9 biological replicates from three independent experiments, *p ≤ 0.01 using two-way ANOVA with Holm-Sidak correction. (e) $[Ca^{2+}]_{mt}$ measurements (mean ± s.d.) in

HeLa expressing the indicated constructs; n = 8 biological replicates (representative of three independent experiments), *p < 0.001 using two-way ANOVA with Holm-Sidak correction. (f) Current traces (left panels) and histograms (right panels) of Mitok together with MITOSUR^{K513A} before and after the addition of 2 mM Mg/ATP (representative of three independent preparations).

Europe PMC Funders Author Manuscripts

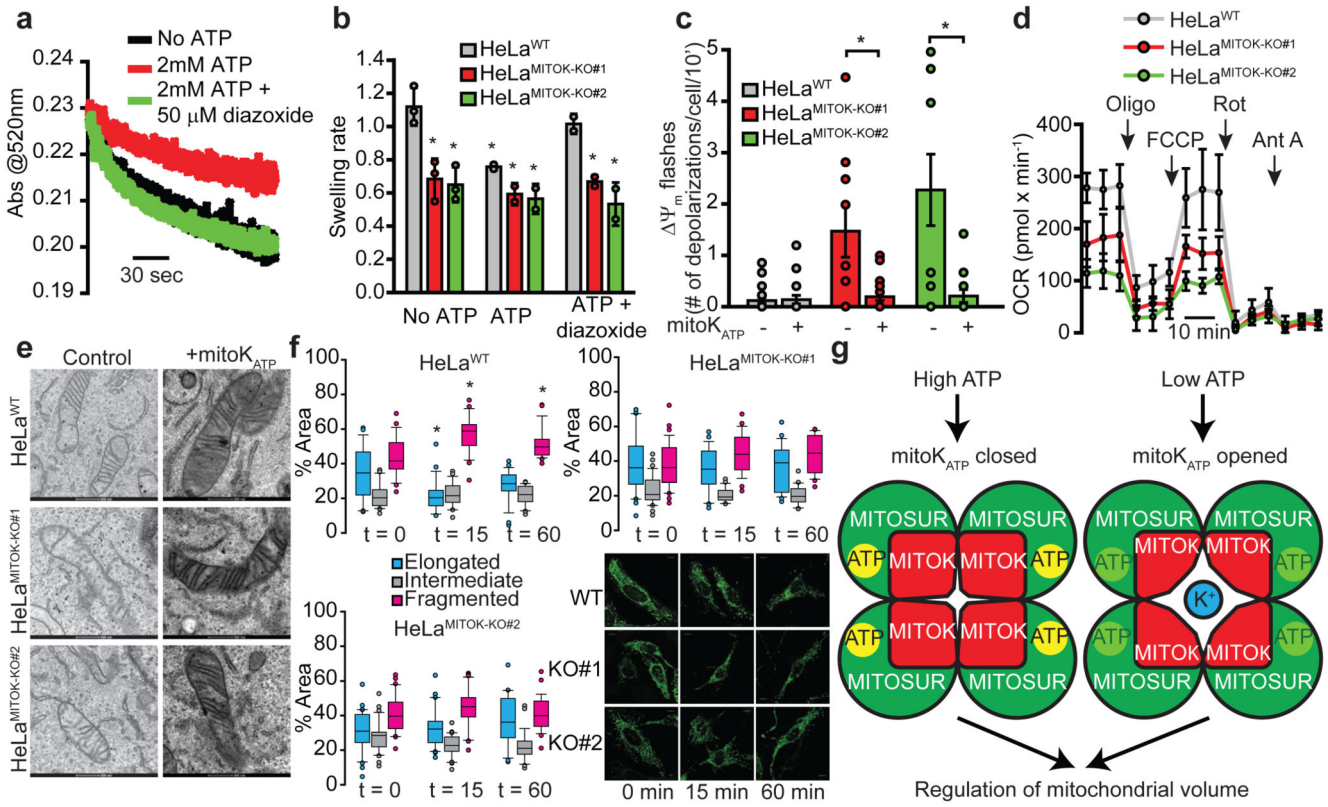

Figure 4. Loss of *MITOK* impairs mitochondrial structure and function.

(a) Swelling traces of wild type mitochondria (three independent experiments with similar results). (b) Mitochondrial swelling rates in K^+-based media. n=2 independent experiments, *p ≤ 0.009 using two-way ANOVA with Holm-Sidak correction. (c) Quantification of $\Delta\psi_m$ flashes. n > 10 independent experiments, *p ≤ 0.001 using two-way ANOVA with Holm-Sidak correction. (d) OCR measurements. n = 5 biological replicates, representative of three independent experiments. (e) TEM images of mitochondrial ultrastructure, representative of two independent preparations. (f) Analysis of mitochondrial morphology during energy stress. Box plots indicated the % of organelle area occupied by elongated (cyan), intermediate (grey) or fragmented (magenta) mitochondria. Scale bars indicate 10μm. n ≥ 22 individual cells from 3 independent experiments, *p < 0.01 using one-way ANOVA with Holm-Sidak correction. (g) Schematic representation of $mitoK_{ATP}$ channels.

Europe PMC Funders Author Manuscripts

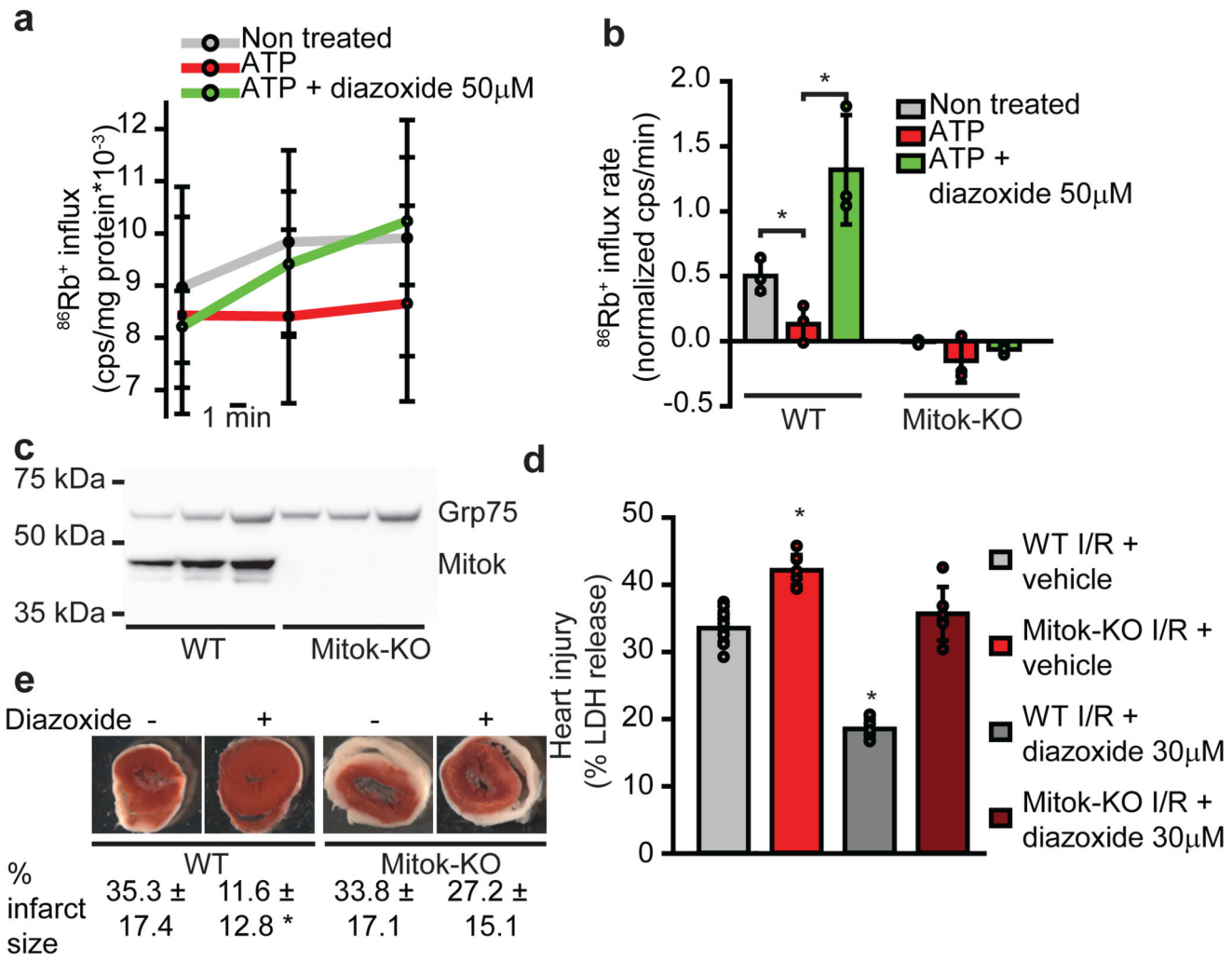

Figure 5. Mitok is required for diazoxide-induced cardioprotection.

(a) $^{86}Rb^{+}$ flux in isolated mitochondria. n = 3 independent experiments. (b) $^{86}Rb^{+}$ uptake rate. n = 3 independent experiments, * $p \leq 0.029$ using two-tailed Student's t-test. (c) Western blot of wt and Mitok-KO liver mitochondria. (d-e) Heart injury after ischemia/reperfusion, evaluated as % of LDH release (d, mean ± s.d., n ≥ 5 independent animals, *$p < 0.001$ using two-way ANOVA with Holm-Sidak correction), or % of infarct area after TTC staining (e, mean ± s.d., n ≥ 7 independent animals *$p = 0.008$). Single measurements are provided in Source Data Tables.